MODELING SCATTERED INTENSITY FROM MICROSPHERES IN AN

EVANESCENT FIELD

A Thesis

by

SUHANI KIRAN SHAH

Submitted to the Office of Graduate Studies of
Texas A&M University
in partial fulfillment of the requirements for the degree of

MASTER OF SCIENCE

December 2007

Major Subject: Biomedical Engineering

MODELING SCATTERED INTENSITY FROM MICROSPHERES IN AN

EVANESCENT FIELD

A Thesis

by

SUHANI KIRAN SHAH

Submitted to the Office of Graduate Studies of
Texas A&M University
in partial fulfillment of the requirements for the degree of

MASTER OF SCIENCE

Approved by:

Chair of Committee,	Kenith Meissner
Committee Members,	Michael Bevan
	Michael McShane
Head of Department,	Gerard Cote

December 2007

Major Subject: Biomedical Engineering

ABSTRACT

Modeling Scattered Intensities from Microspheres

in an Evanescent Field. (December 2007)

Suhani Kiran Shah, B.Eng., Nirma Institute of Technology, Gujarat University

Chair of Advisory Committee: Dr. Kenith Meissner

The technique of single particle Total Internal Reflection Microscopy (TIRM) has been used to study the scattering intensity from levitated microspheres. TIRM can be used to monitor the separation between microscopic spheres immersed in liquid (water in our case) and a surface with nm resolution. In the technique, microspheres scatter light when the evanescent waves are incident upon them. The intensity of the scattered light is directly related to the height above the surface and allows determination of the height. From the separation distance histograms, the interaction between the microsphere and interface may be characterized with a force resolution in the range of 0.01 picoNewtons. Such a system can be applied to the measurement of biomolecular interactions biomolecules attached to the microsphere and the surface. The intensity and scattering pattern of this light has been modeled using a modified Mie theory which accounts for the evanescent nature of the incident light.

Diffusing Colloidal Probe Microscopy (DCPM) is an extension of the TIRM technique that simultaneously monitors multiple microsphere probes. The use of multiple probes introduces the issue of probe polydispersity. When measured at the surface, a variation in scattered light intensity of nearly one order of magnitude has been

observed from a purchased microsphere sample. Thus the polydisperse collection of microspheres adds significant complexity to the scattered light signal. It is hypothesized that the dependence of the total scattered light intensity on microsphere size accounts for the scattered intensity distribution in a polydisperse microsphere sample. Understanding this variation in the scattered light with microsphere size will allow improved characterization of the microsphere/surface separation. Additionally, larger microspheres have the ability to resonantly confine light and produce spectrally narrow Whispering Gallery Modes (WGMs). It is hypothesized that WGMs may be excited in microspheres with the DCPM system. These modes may be used as a refractometric biosensor with high sensitivity to local refractive index changes on the surface of the microsphere.

This research involves modeling scattered intensity distributions for polydispersed collections of microspheres based on modified Mie theory. The theoretical results are compared to experimentally obtained results and found to qualitatively explain the scattered light intensity distribution in a multiple probe DCPM system. This is an important result suggesting that microsphere size variation plays a major role in determining the distribution of scattered intensity in multiple microsphere probe systems. This work also suggests that it may be possible to excite such WGMs in a DCPM system. The introduction of WGMs would enable refractometric biosensing in such evanescent mode systems.

DEDICATION

To my dearest grandmother and family

ACKNOWLEDGEMENTS

I am extremely grateful to my advisor, Dr. Meissner, who has helped me through my Master's. His warmth and guidance was unmatchable. I have learned many things from him; one of which is my presentation skills which have improved a lot. I am also thankful to committee members Dr. Bevan and Dr. McShane. Dr. Bevan and Hung-Jen Wu have been very kind to solve all my queries related to the research work.

I would like to thank my Lab mates, especially Shuo Pang for sharing his knowledge with me and helping me better understand things. Dr. Fink has supported me financially and it is because of him that I had an opportunity to learn a number of things while working on his project.

My parents and my brother have always been with me. They have motivated me in all my endeavors. At times when I was not getting my results, they have always helped me look at the positive side of it. My brother, Samip has amazing skills and has always helped me get a solution to my problems. Finally I would like to thank my friends in College Station who made my stay comfortable here.

TABLE OF CONTENTS

LIST OF FIGURES

LIST OF TABLES

INTRODUCTION

This work investigates the scattered light intensity from levitating microspheres of different sizes when excited by evanescent waves. Evanescent waves are produced in a medium of lower refractive index due to the phenomenon of total internal reflection in a medium of higher refractive index, and decay exponentially with distance above the interface. Because of the spatial variation of the light, microsphere distance from the surface causes variations in the scattered light from microspheres at or near the interface. Single particle Total Internal Reflection Microscopy (TIRM) is a technique which uses this phenomenon to monitor the separation distance between a microsphere immersed in an aqueous solution and the interface with nm resolution. Because it relies on the Brownian motion of the microspheres, TIRM can be used to measure the biomolecular interactions taking place between biomolecules bound to the microsphere and to the interface with sub-picoNewton resolution.

Diffusing Colloidal probe Microscopy (DCPM), developed in the Bevan laboratory, combines TIRM and Video microscopy (VM) to simultaneously monitor multiple microsphere probes. This technique maintains the sensitivity and resolution of single particle TIRM. However, the introduction of a polydisperse sample of microspheres adds greatly to the complexity of the scattered light signal due to variations in microsphere radii.

_____

This thesis follows the style of *Langmuir*.

Understanding these variations in the scattered light with respect to the microsphere size will allow improved characterization of microsphere-surface separation. The intensity and patterns of the scattered light are modeled using modified Mie theory which accounts for evanescent nature of the incident light. All the parameters in the calculations are set to match experimental conditions and there are no free parameters in the calculations.

The scattered intensity from the microsphere is very sensitive to the size and refractive index of the microspheres as well as the effective refractive index of the medium surrounding the microspheres. It is hypothesized that the dependence of the total scattered light intensity on microsphere size accounts for the scattered intensity distribution in a polydisperse microsphere sample. Additionally, larger microspheres have the ability to resonantly confine light through total internal reflection and produce Whispering Gallery Modes (WGMs). These microspheres exhibit a shift in wavelength when the refractive index of the surrounding material or the material inside the cavity changes[1] and may be utilized as refractometric biosensors. It is hypothesized that WGMs may be excited in microspheres with the DCPM system.

In this work scattered intensity values for polydispersed microspheres as observed under DCPM are compared with calculated values using modified Mie theory. From the scattered intensity modeling, the effects of sample polydispersity may be better understood and predicted. It is also found that decay of calculated scattered intensity from a microsphere with distance from the interface matched well with the expected evanescent wave decay. Further, the results suggest that microsphere size variation plays

a major role in determining the distribution of scattered intensity in multiple microsphere probe systems. Finally, the results suggest that it may be possible to excite and use WGMs in a DCPM system.

BACKGROUND

1.   Microspheres

Microspheres are spherical particles with diameters on the order of micrometers. The polystyrene microspheres used in this work are chosen due to their relatively high index of refraction compared to other common microsphere materials (i.e. silica). The value for the index of refraction is calculated at a given wavelength using an empirical fit to data specifically taken on polystyrene microspheres[2]

$$m_{polystyrene} = 1.5725 + \frac{0.0031080}{\lambda^2} + \frac{0.00034779}{\lambda^4} \tag{1}$$

The use of this value will remove all free parameters from the theoretical model. For the investigation into sample polydispersity, polystyrene microsphere samples with mean diameters of 1 and 4 µm are used to compare the modeled light scattering with experimental data.

2.   Evanescent Waves

Evanescent waves are generated at an interface between two materials with different indices of refraction. When light propagating in the higher index material is incident on the interface it is reflected at an angle equal to the incident angle and refracted at an angle described by Snell's law.

$$n \sin \theta_1 = n' \sin \theta_2 \tag{2}$$

where n=high refractive index, n'=low refractive index. It should be noted that the angle of the refracted light, θ_2 is greater than the angle of the incident light, θ_1 due to the lower index of refraction in second material. At the critical angle, the angle of the refracted light θ_2 goes to 90º and the light is totally reflected in the medium in which it is traveling. This angle is defined as[3]

$$\theta_c = \sin^{-1}\left(\frac{n'}{n}\right)$$

(3)

When light is incident at an angle greater than critical angle, total internal reflection (TIR) occurs. Despite the fact that light is not refracted in TIR, light does penetrate the medium of lower refractive index as an evanescent field propagating a short distance along the interface. Most importantly, this light has the property of decaying exponentially with distance from the interface. As shown in figure 1, refractive index of medium 1, n, is greater than medium 2, n'. So, the part of the incident light shown penetrating in medium 2 is an exponentially decaying evanescent wave.
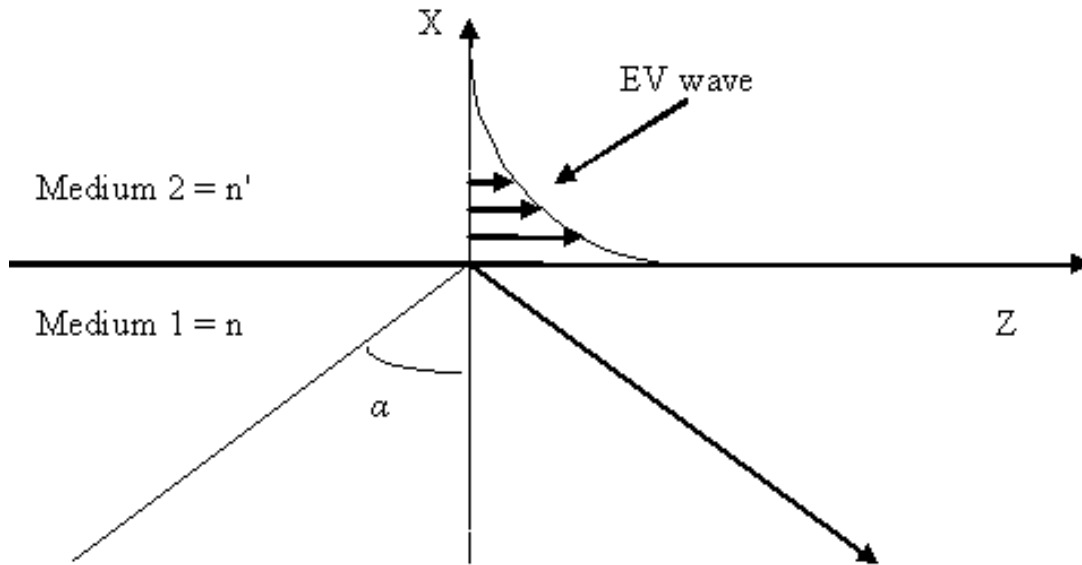
Figure 1 Evanescent wave generation. The evanescent waves are traveling in the direction along Z axis. The refractive index of medium 1 is greater than that of medium 2. α is the incident angle which is greater than critical angle[5].

In this work, the interface is glass and water having refractive indices of 1.515 and 1.33, respectively. Here, the critical angle is 61.38° when the incident light is in the glass. Any angle greater than this critical angle will generate evanescent waves via TIR in the water.

The evanescent wave decay constant in medium 2 is given by following formula[4].

$$\beta = k' \sqrt{\frac{n^2 \sin^2 \alpha}{n'^2} - 1} \tag{4}$$

Here k' is the wave propagation constant of the medium in which the evanescent waves are traveling and is given by the formula:

$$k' = \frac{2 \times \pi}{\lambda} n' \tag{5}$$

β is the decay constant and the inverse of the decay constant gives the penetration depth. The penetration depth is dependent upon the incident angle, the refractive index of medium 1 and the index of medium 2. Thus, the penetration depth may be tuned with incidence angle and gets smaller as the incidence angle increases beyond the critical angle. With an angle of incidence of 68° and refractive indices of 1.33 for water and 1.515 for the glass prism, the depth of penetration is calculated to be 88nm. The evanescent light intensity as a function of distance from the interface is given by[4-6]:

$$I(d) = I_0 \cdot \exp(-\beta v) \tag{6}$$

here, I_0 is the intensity at the water side of the interface and v is the distance from the interface. This evanescent light serves as the source for microsphere scattering in the theoretical model and experiments.

3.   Single Particle TIRM

Incoming incident light from a laser is incident upon the interface at an angle slightly greater than the critical angle. The generated evanescent light produced in the water is incident upon a microsphere which scatters light away from the interface. This scattered light may be collected perpendicular to the interface, along the x-axis, as labeled. The scattered intensity is assumed to be directly related to intensity of evanescent waves and microsphere size as shown in figure 2. Since the intensity of the evanescent wave exponentially decreases as the distance from the surface increases, the scattered intensity is also expected to decrease with distance from the interface and

follow the relation described in equation (6)[7]. Here, I_0 is the scattered intensity when the microsphere is on the surface and d is the distance from the interface to the bottom of the microsphere. Using equation (6), the measured I_0, and the calculated penetration depth, the distance between the sphere and glass interface can be calculated from the scattered intensity. Experimentally, the distance from the interface to a microsphere suspended in water may be monitored. The initial step is to determine I_0 for the microsphere. Due to gravitational force, the relatively dense microsphere comes in close contact with the glass slide[5]. At this point, the microsphere is at a distance 0 above the surface and the base line intensity or "stuck particle' intensity is measured. After establishing I_0, the microsphere is suspended in water above the glass/water interface. It should be noted that the value of I_0 varies significantly between microspheres within a relatively monodisperse sample, this fact was addressed while discussing polydispersity issue with Dr. Bevan. This variation appears to become larger as the microsphere index increases (i.e. from silica to polystyrene).
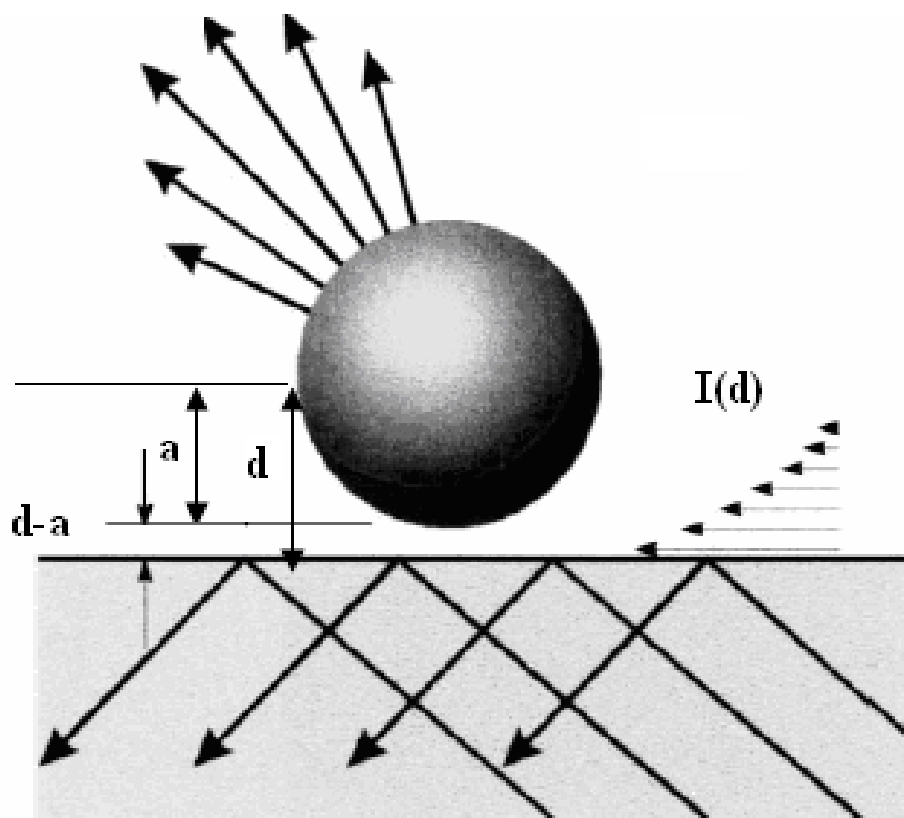
Figure 2 Single particle TIRM. The radius of microsphere is a, and it is located at distance (d-a) from the surface, the distance between the centre of the microsphere and surface is d[8].

Once the microsphere is levitated above the surface, Brownian motion causes the microsphere to continuously change its height above the surface. As shown in the figure below the microsphere is located at distance (d-a) from the surface, d is the distance between the centre of the microsphere and interface, a is the microsphere radius. This change in height is measured as a change in the scattered intensity. This technique is sensitive, since it utilizes Brownian motion to cause the changes in height. A

microsphere height histogram, *n(h)*, can be built from time dependent height fluctuations, *h(t)*, for the microsphere due to Brownian motion as[8]:

$$h(t) \rightarrow n(h) \tag{7}$$

Then, a probability density function given by the following formula can be substituted for *n(h)*[8]

$$p(h) = A \exp\left[-\frac{\phi(h)}{k_B T} \right] \tag{8}$$

Here, *p(h)* is the probability of sampling height above the glass surface, $\varphi(h)$ is the microsphere and surface potential energy profile, A is a normalization constant, $k_B T$ is the thermal energy.

Ensemble averaging can then be used to determine the reference height or the most probable height, h_m, which is then taken into account as a reference for further calculations. Now, the potential energy relative to the reference height can be given by following expression[8]

$$\frac{\varphi(h) - \varphi(h_{ref})}{k_B T} = \ln\left[\frac{n(h_{ref})}{n(h)} \right] \tag{9}$$

here, h_{ref} = most probable height or the reference height, $\varphi(h_{ref})$ = potential energy of the sample at corresponding reference height, *n(h)* = histograms providing good approximation of the probability density of heights *p(h)*. Thus distances calculated between the microsphere and surface directly corresponds to the interaction between the glass surface and the microsphere. Thus it is possible to study biomolecular interactions between biomolecules attached to the surface of the microsphere and on the surface of

the glass slide. This technique allows derivation of forces acting on the microsphere with kT resolution and can be utilized to characterize the interaction between biomolecules. TIRM is a very sensitive technique and it measures force non- intrusively. Thus with the help of TIRM we can measure forces in the sub-picoNewton range[9]. Liebert and Prieve used TIRM to measure specific interactions between immunoglobulin G (IgG) covalently bound to a polystyrene microsphere and protein A covalently bound to the glass slide[10]. Robertson et al. measured the potential energy of interaction between a glass interface and a leukocyte at very low ionic strengths[11]. Robertson and Bike have used TIRM to measure non-specific, interactions between biomolecules and a glass surface. These interactions play an important role in controlling the adhesion of cells and liposomes to surfaces[12]. Rudhardt et al. used TIRM to measure the depletion interactions between polystyrene microspheres and a glass interface in the presence of poly (ethylene oxide) (PEO)[13, 14].

4.   TIRM Compared to Other Techniques

The primary force measurement techniques currently being used for biomolecular measurements are atomic force microscopy (AFM) and optical tweezers. More recently developed, TIRM offers an alternative method with some advantages over the traditional techniques. This technique has shown that the force sensitivity is two order higher in magnitude than Atomic Force Microscopy (AFM)[5].

AFM is a tool for directly measuring force in the pN range and imaging matter at nanometer scales. When characterizing force, the AFM operates by measuring attractive or repulsive forces between the tip and a sample[15]. Two types of biomolecular forces are

normally measured; the binding and unbinding forces between the biomolecules. The unbinding forces are more easily measured through rupture force measurement. For measuring the unbinding forces with AFM, a cantilever with a sharp, biofunctionalized tip is used. The cantilever is scanned across the sample and comes in contact with the sample of interest. Interaction between the biofunctionalized tip and the sample causes deflection of the cantilever and the deflection is measured by the change in a reflected laser beam detected with a photodetector. From these distances and the stiffness of cantilever, the forces acting between the biofunctionalized tip and sample are calculated through Hooke's Law[16]:

$$F = -k \times d,$$
(10)

Here, F is the force measured, k is the stiffness of the cantilever and d is the distance measured by the deflection of cantilever.

This ability of AFM to measure discrete intermolecular forces has been exploited by many research groups for biomolecular force measurement. Jeong and group worked on detecting direct force measurement between biotin attached to a 10 μm polystyrene bead and streptavidin on the surface[17]. The forces measured were in the range of hundreds of picoNewtons, 636±176 pN[17]. Allen and group worked on detecting the unbinding forces between ferritin antigen and anti ferritin antibody attached to the AFM probe and surface in contact respectively. The precise forces in the range of 49±10pN were measured[18]. Lee and group measured the forces between complementary strands of DNA. The forces measured were in the range of nano Newtons[19].

Optical tweezers use the force of radiation from a focused laser to trap small particles on the order of nano- to micro-meters[20]. The trap functions on transparent particles with an index of refraction that is greater than the surrounding media. Stable trapping is achieved when the gradient force is larger than the scattering force. The forces acting on the trapped sphere can be calculated from the amount of displacement it undergoes from the focal point. This technique is utilized in measuring the interaction and adhesion between the biological samples attached to microspheres. The forces on the order of 1 to 100 pN have been characterized[21]. The principle of force calculation is similar to that mentioned for AFM. Tinoco and group calculated the forces acting on the RNA from the distance between microbeads. Their paper describes a review on the use of optical traps for understanding the mechanisms of folding and unfolding of RNAs[22]. Finer and group used laser trap that allowed for direct force and displacement measurement that results from interaction of a single myosin molecule with a single suspended actin filament, the forces measured were around 3 to 4 pN and distances of 11 nm[23]. The system developed by Fallman and group has been used to measure the binding forces between Escherichia coli bacterial adhesins and galabiose-functionalized beads. The binding between the biomolecules ruptured at the forces of 10-15 pN[24].

TIRM offers a number of advantages compared to traditional techniques for measuring biomolecular interactions. The following table summarizes the various advantages and disadvantages of the techniques discussed above[25]:

Table 1 Summary of comparison between the techniques

Technique	Advantages	Disadvantages
AFM	1) Direct force measurement, 2) technique works in air or liquid, 3) provides high resolution imaging in addition to force information[26]	1)Requires chemical or physical immobilization of the biomolecules when measurements are made in liquids, 2) No absolute measurement of distance so calibration is required, 3) Maximum force measured is in range on pN 4) Physically touches the sample and might transfer energy to sample[27]
Optical Tweezers	1) No immobilization required, 2) works best for spherical particles 3) light must pass through the trapped particle[20, 28]	1) Valid over very narrow particle range 2) Maximum force measured is in range on pN
TIRM	1) Forces as small as 10^{-14}–10^{-10} N can be resolved 2) Distances between the particle and surface can be	1) Low refractive indices and flexible membranes hamper the practical use of TIRM on cells. 2) Biomolecules should be labeled

	measured directly[9, 29]	fluorescently for imaging purpose[9]

5.   MIE Theory

In order to model light interactions with spherical particles, Mie theory is traditionally used. Mie theory was independently developed by Gustav Mie[30] and Ludvig Lorenz. Mie theory provides a complete mathematical solution for scattering of electromagnetic radiation from spherical particles[3]. Mie theory is well described in numerous texts including those by Bohren and Huffman[31], Kerker and van de Hulst[32].

Two parameters important for the calculations in Mie theory are size parameter, $x,$ and effective refractive index, $n_{eff,}$ The size parameter of the spherical particle is defined by the following formula

$$x = k'a = \frac{2\pi a}{\lambda} n'$$ (11)

where k' is the wave number of the medium in which waves are propagating, λ is the wavelength of the incident incoming light, a is the microsphere radius, n' is the refractive index of the medium surrounding the microsphere. The size parameter gives the idea that when the microsphere size is more or the wavelength of incident light is less the size parameter will be more and more the size parameter more is the light scattered from them. The effective refractive index is given by:

$$n_{eff} = \frac{n_1}{n'}$$ (12)

where, n_1 and n' are the refractive indices of microsphere and of the medium surrounding the microsphere, respectively. This parameter shows the amount of contrast or confinement provided by the particle. These two parameters are very sensitive. Small shift in them can cause a large change in the value of the scattered intensity as will be seen in the results and discussion section.

Mie theory makes the following assumptions[5]:

1) The microspheres are assumed to be homogeneous, made up of linear and isotropic materials.

2) Each microsphere is assumed to be located in an infinite homogeneous, lossless medium (AT).

3) The incident light is assumed to be continuous and an infinite plane wave.

The first two assumptions match well with the system under investigation. However, the final assumption is not acceptable for our system. Hence, Mie theory is not directly applicable for the theoretical calculations. Thus, modified Mie theory which accounts for the evanescent nature of the source light is required in our calculations.

The first treatment of scattering problem with modified Mie theory was presented by Chew et. al[6]. They calculated the scattered light from a 1 μm diameter microsphere in air with plane wave as well as evanescent wave excitation using Mie and modified Mie theory, respectively. The results showed scattered light intensity from evanescent excitation differed significantly from that of plane wave excitation. Additionally, the angular scattering pattern and the total amount of scattered light were found to depend upon the size of the microsphere, the penetration depth of the evanescent light, the

polarization of the light, and the distance of microsphere from the interface[33]. Due to assumptions made to decrease computational time, the calculated results hold in two principal planes. Recently, Ganic et. al[7] solved the scattering of the microspheres of particle radius 2 μm in air with evanescent wave excitation and calculated the three dimensional scattering from the sphere using the modified Mie theory based on the work of Chew et al. They looked theoretically at the resonant modes occurring in the pattern of the scattered intensity, and they attributed sharp peaks occurring in this process as morphology dependent resonances (MDRs). This theoretical model is used in this work and is described in detail in theoretical methods section.

6.   Diffusing Colloidal Probe Microscopy

As shown above, single particle TIRM is useful for characterizing particle/surface or biomolecular interactions. However, the technique may be extended by the simultaneous use of multiple microsphere probes. By multiplexing an ensemble of microsphere probes, the system can measure many interactions at once to provide a more complete experimental picture. Dr. Bevan's lab has recently combined TIRM and Video Microscopy (VM) to simultaneously monitor the activity of multiple microsphere probes.
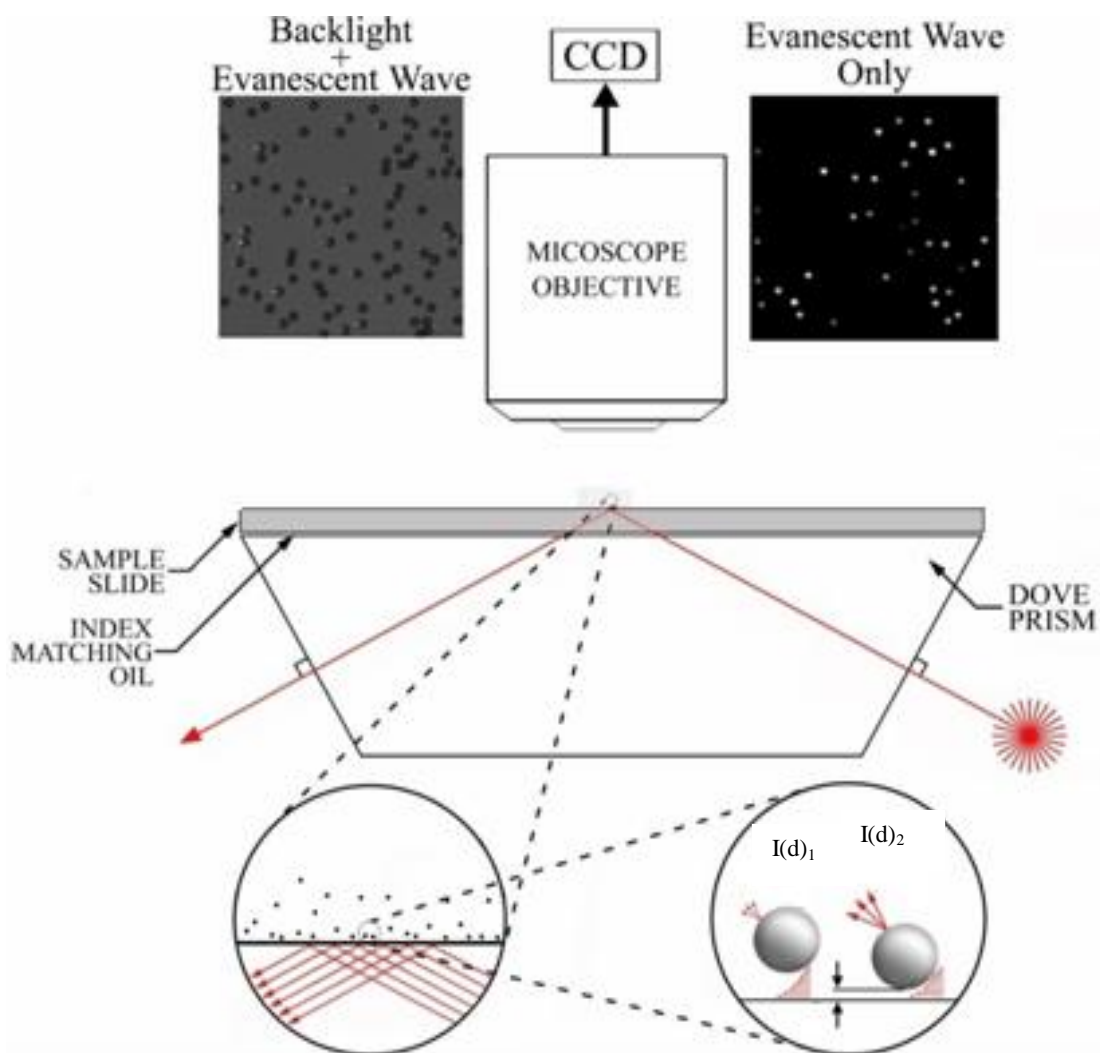
Figure 3 DCPM system for multiple particles. The laser light is incident on the prism from the right, the evanescent waves are generated above the slide and the microsphere sample on the slide is illuminated by these waves. The inset shows the microspheres of different sizes located at different distances above the slide. The images shown in above the setup is the different patterns of the microsphere scattering, the images are captured by CCD.

This system is referred to as diffusing colloidal probe microscopy (DCPM) and is shown in the figure 3. Just as TIRM uses a single probe, DCPM is used to simultaneously monitor scattered light from an ensemble of microsphere probes.   From these measurements, the microsphere height distribution and eventually the microsphere/surface interaction may be calculated.

The simultaneous use of multiple microspheres introduces issues of microsphere polydispersity. As shown in figure 3, courtesy Dr. Bevan and group, the microsphere sample dispersed in water sits on the glass slide above the prism and as described before evanescent waves produced are incident upon them and they scatter light. This scattered light is captured by the CCD camera and the images appear as shown in the figure. The right image is taken when the backlight is off and left is the image with backlight. In the left image we can distinctly see the differences in microsphere size, and those microspheres do not emit the same amount of light. This effect is possibly due to the distance between the microsphere and surface, differences in microsphere size or changes in refractive index. The insets below the main figure are cartoons showing a sample of microspheres dispersed in water and how the microspheres at different heights scatter light differently. The work by Chew and Kerker demonstrated that this scatter may be due to both microsphere/surface distance and also microspheres size[6]. This work investigates the effect of microsphere polydispersity on the distribution of scattered light intensity as a function of microsphere size.

DCPM maintains the sensitivity and resolution similar to that of single particle TIRM, with the advantage of simultaneous probing by multiple microspheres. Hence the

time required for calculation decreases. For the study of biomolecular interactions for multiple particles, Everett et al have looked at interactions of BSA adsorbed microspheres and its interaction with copolymer PEO attached to a glass slide with DCPM[34]. The data in the paper show distinct improvement of measuring simultaneous microspheres together rather than measuring the data for each single microsphere and then averaging it[34]. Thus DCPM is a new technique to measure biomolecular interactions with kT resolution.

7.   Whispering Gallery Modes

When light is confined inside the microsphere due to the phenomenon of TIR, the resonant modes generated are called Morphology Dependent Resonances or Whispering Gallery Modes (WGMs). These resonance modes are critically dependent upon the size and refractive of the microsphere, and the local refractive index of medium surrounding the microsphere. For a given microsphere, these modes occur at particular resonant wavelengths of light and may be very sharp with quality factors (Q) up to 10,000: where Q equals the center frequency divided by the frequency bandwidth[35]. As shown in the figure 4, when light is coupled inside the microsphere, it undergoes constructive interference as it undergoes TIR and circulates near the surface of the microsphere. These modes have a wide variety of applications as filters, lasers, sensors and modulators[36]. The scattering intensity pattern of the microsphere when coupled in a WGM differs distinctly from the normal scattering pattern which we will see in the result section. The enhanced scattering characteristics provide good information for the fields of microscopy and optical sensing[37]. These modes have high Quality (Q) factor,

which we will discuss in the section of mode sensing[36]. Due to the high Q of these resonant modes, microsphere WGMs may be used for refractometric biosensors[35, 38, 39].
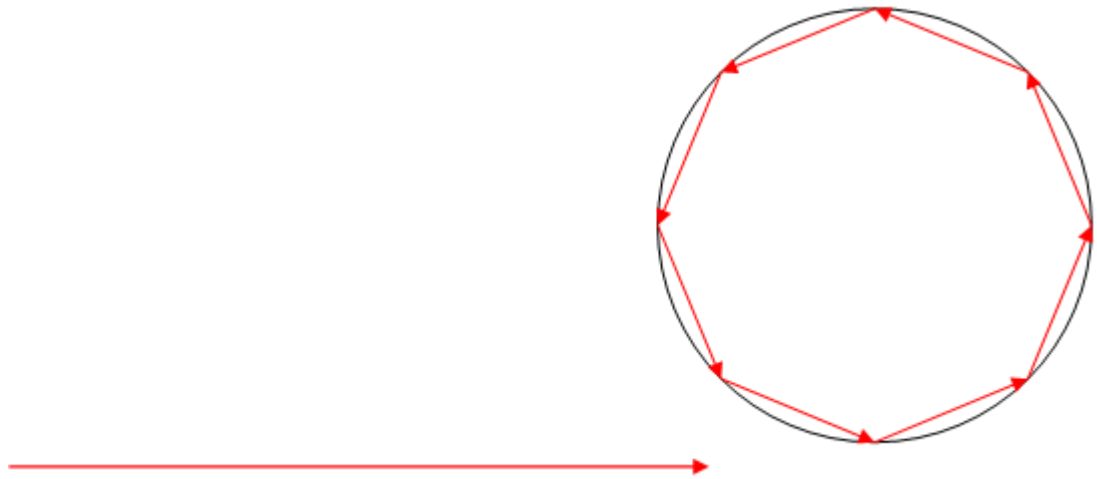
Figure 4 Whispering Gallery Modes (WGM) resonances occur due to TIR on the inner surface of the microsphere. They are efficiently excited with evanescent light due to the high angle of incidence near the bottom of the microsphere.

8.   WGM Biosensing

Due to the evanescent tail of the WGMs extending into the surrounding medium, the resonant frequencies, or wavelengths, of these WGMs are extremely sensitive to the refractive index near the microsphere surface. Thus by attaching biomolecules to the surface of these microsphere, the system may be used as a biosensor. Adsorption of biomolecules on the surface of the WGM microsphere sensors results in a change in the effective refractive index of the surrounding medium and may lead to a measurable shift in resonance wavelength. Examples of potential applications for WGM microsphere

biosensors include detection and monitoring of proteins, DNA, peptides and toxin molecules[40]

The system senses changes in the refractive index of the medium directly surrounding the microsphere, n', due to the attachment of biomolecules. Since the mode generally remains at a fixed value of the size parameter, x, sensing is accomplished through the observation of wavelength shifts in the resonant WGMs as n' changes. Due to minimal losses, the WGM resonances may possess very high Quality factors: the parameter that indicates the strength of resonance modes coupled inside the microspheres. So to improve measurement precision, the narrow mode linewidth achieved from high Q factor may be used[35]. Q factor is defined as[41]:

$$Q = \frac{\omega_0}{\Delta\omega}$$

(13)

where, $\Delta\omega$ is the resonance linewidth here and ω_0 is the resonant frequency. The results of change in wavelength are dependent upon the Q factor and the microsphere radius greatly influences the value[35].

It has been shown that when the effective refractive index increases due to adsorption of a protein, DNA or the peptides on the surface of a microsphere, the the resonance frequency will decrease or the resonance wavelength will increase[40]. So, the size parameter of the microsphere, as defined in the mie section always remains fixed. But due to the change in refractive index of the medium surrounding the microsphere, the value is to be manipulated in a way that size parameter remains constant. And

change in wavelength is possible if we have incoming light coming from a tunable laser at different wavelengths.

Using this concept it has been shown that different proteins when attached to the WGM biosensors, induce different wavelength shifts[42]. The ratio of wavelength shift due to streptavidin binding compared to BSA biotin adsorption was 0.94. It is also shown that due to the addition of new materials on the surface the wavelength shifted to longer values to accommodate a larger effective circumference[42].

Arnold et al showed that single molecule detection on the surface may be possible through the use of WGM biosensors[38]. They used BSA (Bovine Serum Albumin) and a perturbation approach for analyzing the resonance shift, and showed that the shift in the frequency is inversely proportional to the microsphere radius. Vollmer et al quantified DNA attached to the surfaces of two microspheres together and found the fractional wavelength shift for a single DNA molecule[43]. In the latest paper by Quan and Guo, a refractive index change of 10^{-5} is distinguishable by a WGM biosensor when a linewidth of 10 MHz is considered[40]. They also showed that WGM biosensors can measure the adsorption and growth of one single peptide layer. When the peptides started to grow on the surface of a 30 μm diameter WGM biosensor, the wavelength was downshifted. They found a linear relationship between the peptide thickness and the absolute value of the decrement of resonance wavelength[40].

SOLUTION

1. Modified MIE Theory

Due to the basic assumptions of Mie scattering, the technique is not applicable to DCPM experiments. Thus, basic Mie theory must be modified to account for the evanescent nature of the incoming incident light. The implementation of the modified Mie theory used in this work is based on the earlier work by Chew and Kerker[6] but does not contain the limitations restricting results to the principle planes[7]. The scattered evanescent field from the microspheres is given in spherical coordinates as:

$$E_{sc}(r) = \sum_{lm}\left\{\frac{ic}{n'^2\omega}\beta_E(l,m)\nabla\times\left[h_l^{(1)}(k'r)Y_{llm}(\hat{r})\right]+\beta_M(l,m)h_l^{(1)}(k'r)Y_{llm}(\hat{r})\right\} \tag{14}$$

Here l is the radial mode number and m is the azimuthal mode number, $h_l^{(1)}(k'r)$ are spherical hankel functions of the first order, $\beta_M(l,m)$ and $\beta_E(l,m)$ are the scattered field expansion coefficients, ω is the angular frequency of the light, c is the velocity of light in vacuum, Y_{llm} are the vector spherical harmonics, n′ is the refractive index of the surrounding medium, k′ is the wave number of the medium in which waves are propagating, and r is the radial spherical coordinate. To simplify equation 9, the del function required in the spherical coordinates,

$$\nabla\times\left[h_l^{(1)}(k'r)Y_{llm}(\hat{r})\right] \tag{15}$$

is calculated from the simplified form as shown below. Let A be the simplified vector field

$$A_r(\hat{r})+A_\theta(\hat{\theta})+A_\varphi(\hat{\varphi}) \tag{16}$$

Curl of vector field A is given by the following formula

$$\nabla \times A = \frac{1}{r\sin\theta}\left(\frac{\partial}{\partial\theta}\left(A_\varphi\sin\theta\right)-\frac{\partial A_\theta}{\partial\varphi}\right)\hat{r}+\frac{1}{r}\left(\frac{1}{\sin\theta}\frac{\partial A_r}{\partial\varphi}-\frac{\partial}{\partial r}\left(rA_\varphi\right)\right)\hat{\theta}+\frac{1}{r}\left(\frac{\partial}{\partial r}\left(rA_\theta\right)-\frac{\partial A_r}{\partial\theta}\right)\hat{\varphi}$$

(17)

Vector spherical harmonics can be simplified further, with the help of following equation in spherical coordinates[44]

$$\sqrt{l(l+1)}Y_{l,l}^m = i1_\theta\csc\theta\partial_\varphi Y_l^m - i1_\varphi\partial_\theta Y_l^m$$

(18)

where spherical harmonics required for the expansion of the plane wave are generalized by Y_{llm}, vector spherical harmonic. The vector spherical harmonics are expanded and they are given as shown in the equation 18. The expansion consists of scalar spherical harmonics given as Y_{lm}.

Substituting equations (16) and (17) into equation (14), and solving for the unit spherical vectors of r_1, θ_1 and φ_1 gives the expansion of the formula for the scattered field in spherical coordinates as given in equation[7] (19)

$$E_{sc}(r)=\sum_{lm}\left\{\begin{array}{l}\dfrac{c\beta_E(l,m)}{n'^2\,\omega\sqrt{l(l+1)}}\dfrac{h_l^{(1)}(k'r)}{r\sin\theta}\left[\dfrac{\partial}{\partial\theta}\left(\dfrac{\partial Y_{lm}\sin\theta}{\partial\theta}\right)+\dfrac{1}{\sin\theta}\dfrac{\partial^2 Y_{lm}}{\partial\varphi^2}\right]r_1\\[4mm]+\left[\dfrac{(-1)\beta_M(l,m)h_l^{(1)}(k'r)}{i\sin\theta\sqrt{l(l+1)}}\dfrac{\partial Y_{lm}}{\partial\varphi}-\dfrac{c\beta_E(l,m)}{n'^2\,\omega\sqrt{l(l+1)}}\dfrac{1}{r}\dfrac{\partial Y_{lm}}{\partial\theta}\dfrac{\partial}{\partial r}\left(rh_l^{(1)}(k'r)\right)\right]\theta_1\\[4mm]+\left[\dfrac{\beta_M(l,m)h_l^{(1)}(k'r)}{i\sqrt{l(l+1)}}\dfrac{\partial Y_{lm}}{\partial\theta}-\dfrac{c\beta_E(l,m)}{n'^2\,\omega\sqrt{l(l+1)}}\dfrac{1}{r\sin\theta}\dfrac{\partial Y_{lm}}{\partial\varphi}\dfrac{\partial}{\partial r}\left(rh_l^{(1)}(k'r)\right)\right]\varphi_1\end{array}\right\}$$

(19)

where r_1, θ_1, φ_1 are the unit vectors in spherical coordinates, k' is the wave number in the medium, r is the radial spherical coordinate, Y_{lm} are the scalar spherical harmonic function of degree l and order m respectively, l and m are the redial mode numbers and azimuthal mode numbers respectively ($l = 1$ to ∞ and $m = -l$ to $+l$), $\beta_M(l,m)$ and $\beta_E(l,m)$ for transverse magnetic and transverse electric mode respectively are the scattered field expansion coefficients required to expand electromagnetic plane waves in spherical harmonics, c is the velocity of light in vacuum, $h_l^{(1)}(k'r)$ are the Hankel functions of the first kind, ω is the angular frequency of the light. To calculate the scattered field using the equation (19), the equation is summed over modes, l, until the contribution becomes negligible. This equation holds true for the incident electric wave E_0 is perpendicular to the plane of incidence (i.e. for the S polarized waves).

2. Significance of Expansion Coefficients

The primary modification to Mie theory for evanescent wave excitation comes in the scattered field expansion coefficients given by[6]:

$$\beta_E(l,m) = \frac{\left[\varepsilon' j_l(k'a)[k_1 a j_l(k_1 a)]' - \varepsilon_1 j_l(k_1 a)[k'a j_l(k'a)]'\right]\exp(-\beta d)\alpha_E(l,m)}{\varepsilon_1 j_l(k_1 a)[k'a h_l^{(1)}(k'a)]' - \varepsilon' h_l^{(1)}(k'a)[k_1 a j_l(k_1 a)]'} \tag{20}$$

$$\beta_M(l,m) = \frac{\left[\mu_1 j_l(k_1 a)[k'a j_l(k'a)]' - \mu j_l(k'a)[k_1 a j_l(k_1 a)]'\right]\exp(-\beta d)\alpha_M(l,m)}{\mu' h_l^{(1)}(k'a)[k_1 a j_l(k_1 a)]' - \mu_1 j_l(k_1 a)[k'a h_l^{(1)}(k'a)]'} \tag{21}$$

Where, μ, ε, and k are the magnetic permeability, dielectric constant and wave number for the glass prism, μ_1, ε_1, and k_1 are the magnetic permeability, dielectric constant and

wave number for the medium surrounding the sphere, μ', ε', and k' are the magnetic

permeability, dielectric constant and wave number of the sphere, β is the decay constant

of the evanescent wave, $j_l(ka)$ are the spherical Bessel functions of the first order.

$\alpha_M(l,m)$ and $\alpha_E(l,m)$ are the expansion coefficients of the incident field for transverse

magnetic and transverse electric modes respectively, d is the distance between the

microsphere centre and the glass surface, a is the microsphere radius. The expansion

coefficients also contain an exponent decay with distance from the surface.

$\alpha_E(l,m)$ and $\alpha_M(l,m)$ are as defined below[6]

$$\alpha_E(l,m) = 2mi^l n' \sqrt{\left(\frac{\pi(2l+1)(l-m)!}{l(l+1)(l+m)!}\right)} \left[\frac{P_l^m(\cos\theta_{k'})}{\sin\theta_{k'}}\right] * E_0' \tag{22}$$

$$\alpha_M(l,m) = -2i^{l+1} \sqrt{\frac{\pi(2l+1)(l-m)!}{l(l+1)(l+m)!}} \left[\frac{d}{d\theta_{k'}} P_l^m(\cos\theta_{k'})\right] * E_0' \tag{23}$$

Here, P_l^m is the associated Legendre's Polynomial, $\theta_{k'}$ is the complex angle of incidence

calculated from the critical angle 61.38º for glass water interface, to match the

experimental conditions and for TIR we took 68º, for which the complex angle

calculated is $\theta_{k'}$. In our case the complex angle is taken as (0, 0.36663). The amplitude of

the refracted wave is given by the following formula:

$$E_0' = \frac{2}{1 + \frac{\mu\tan\alpha}{\mu'\tan\alpha'}} \tag{24}$$

The expansion coefficients are functions of the size parameter of the

microsphere. And the size parameter as defined in the mie section are in turn dependent

on the microsphere radius a and refractive index of the medium. Thus, the scattered field

is very sensitive to changes in these parameters. It should be noted that larger microspheres require more spherical harmonic modes to reproduce the initial plane wave excitation and convergent results.

In summary, modified Mie theory used here takes into consideration the evanescent nature of the incident light. It also indicates that the size of the microsphere influences the amount of light scattered in a complex manner. This work will explore this relationship to explain the variation in scattered light observed from polydisperse microsphere samples.

METHODS

1.   Experimental Method

DCPM experiments were performed by the Bevan Laboratory. Excitation was provided by the 488 nm line from an Argon Ion laser (Melles Griot, Carlsbad, CA). The light is normally incident on the side face of a Dove prism with the sides cut at 68º. This yields the incidence angle of 68º and the laser is set to perpendicular, or S, polarization. For the glass-water interface, Corning glass slides (Corning, NY) were used for all the experiments and optically coupled to the prism with index matching oil (n=1.515). The slides were washed for 30 minutes in Nochromix (Godax Laboratories, Takoma park, MD), rinsed repeatedly with double deionized water (DDI), and dried thoroughly with high purity nitrogen. O-rings, 10mm ID $\times$ 12mm OD, (Viton, McMaster Carr, Los Angeles, CA) were used to form two samples on each slide. The microspheres with mean diameters of 1, and 4 µm were purchased from Interfacial Dynamics Cooperation (Eugene, OR). Microsphere samples were diluted with DI water to create low concentration samples for the experiments. Dynamic light scattering was used to measure the microsphere size distributions (ZetaPALS, Brookhaven Instrument Corporation, Holtsville, NY). The schematic representation of the actual setup is shown in figure 4 from the DCPM section above. An Axioplane 2 optical microscope (Zeiss, Germany) with a 40X objective lens (NA = 0.6) was used to collect the scattered intensity. A 12-bit CCD camera (ORCA-ER, Hamamatsu, Japan) operated with 2x binning and a capture rate of 18 frames/second was used to record the scattered light from the microspheres. Images contained 672 pixels x 512 pixels, had a pixel resolution

of 304 nm and yielded an image field of 204 x 155 μm^2. The image shown in figure 5 (a), courtesy Dr. Bevan and group, is of polydispersed microspheres scattering light when the evanescent waves are incident on the microspheres from the right side. Hence we see a bright illumination on the right side which is forward scattering and a very low backward scattering as well.
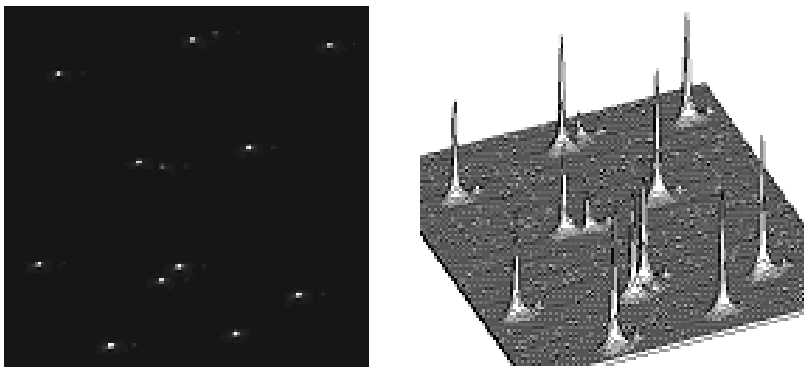

Figure 5 (a) Shows the evanescent wave scattering intensities profiles of 4 μm single PS microspheres.
Figure 5 (b) Shows the scattering image corresponding to (a) recorded from the optical microscope.

Image analysis algorithm and software code coded in FORTRAN were used to track the location of the microspheres and record the scattered intensity. To locate and track evanescent wave signal on each of the microsphers, standard video microscopy algorithms were used[45, 46]. The total scattered intensity from individual microspheres was calculated as the integrated sum for each of the pixels falling in a specified radius around each microsphere. Only isolated microspheres are tracked to prevent cross-talk. These

intensities are recorded as a function of time and yield the height distributions for each microsphere.

2.   Theoretical Calculation

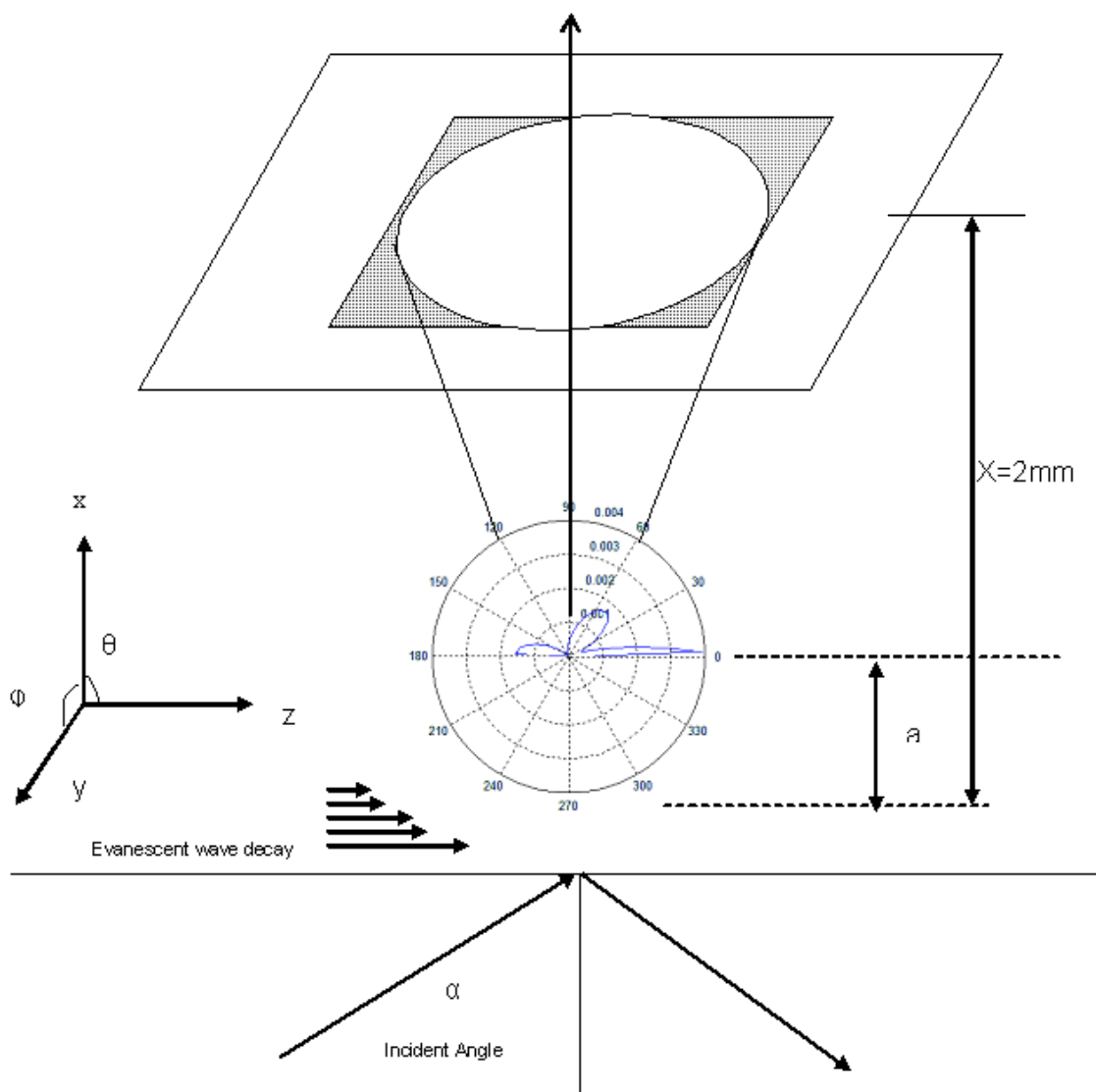Figure 6 Model configuration for theoretical calculations showing the axis. Here evanescent waves travel along Z axis, the size of the microsphere chosen for the polar plot is 4 μm diameters PS. The light is scattered more in the forward direction and hence higher values of scattered intensity at around 0˚. A weak lobe also occurs at the end near 180˚, which can be mainly attributed to backward scattering.

The software code used to calculate the scattered light is a modified version of code previously used to study evanescent wave scattering from microspheres by Ganic et al[7]. To increase computational speed, the program is written in FORTRAN 77. Figure 6 shows the configuration for the theoretical calculations. In this work, the scattered light distribution is calculated at a YZ plane located above the interface. Parameters set in the code included:

- The wavelength of incident light from Argon Ion laser: 488 nm

- The angle of incidence: 68º

- Refractive index of water: 1.33

- Refractive index of glass prism: 1.515

- Index of refraction for polystyrene microsphere: 1.59168

- Polarization of the light: perpendicular

The working distance of the 40x objective used to collect the scattered light determines distance to the YZ collection plane: 2mm in this case. The numerical aperture of the 40x objective determines the angular collection cone: approximately 30º in this case. Thus, the collection angle varies between 60º and 120º in θ and between -30º and 30º in φ. The light distribution is calculated for equal steps across the defined circular collection area in the YZ plane in order to keep the individual collection area segments constant. For each step, the values for r, θ, and φ are determined which in turn are used to determine the scattered intensity in that area element. The scattered intensity from all area elements are then summed to find the total scattered intensity.

Experimental measurements showed that the polydispersed polystyrene microsphere sample of diameter 1 spanned the range from 0.6 µm to 1.4 µm and 4 µm particle spanned the range from 2.5 µm to 4.5 µm Thus, calculations were performed over the range between 0.25 µm radius to 2.5 µm for including all the sizes required for 1 and 4 µm sample. The step size in the YZ collection plane in this size range was 5 nm. For larger microspheres, the peaks become sharper and frequent and so to capture all the values required, we should chose a still smaller step size.

Figure 7 below is the plot of microsphere radius versus the scattered intensity. The peak at about 2.45 µm is the narrowest peak in these calculations. This peak is well defined by the 5nm step size and hence the step size of 5 nm was chosen for 2 and 4 µm diameter microspheres. Also to be noted here that the broad peaks in the earlier portion of this curve for small microspheres are very well defined with the step size of 5 nm.
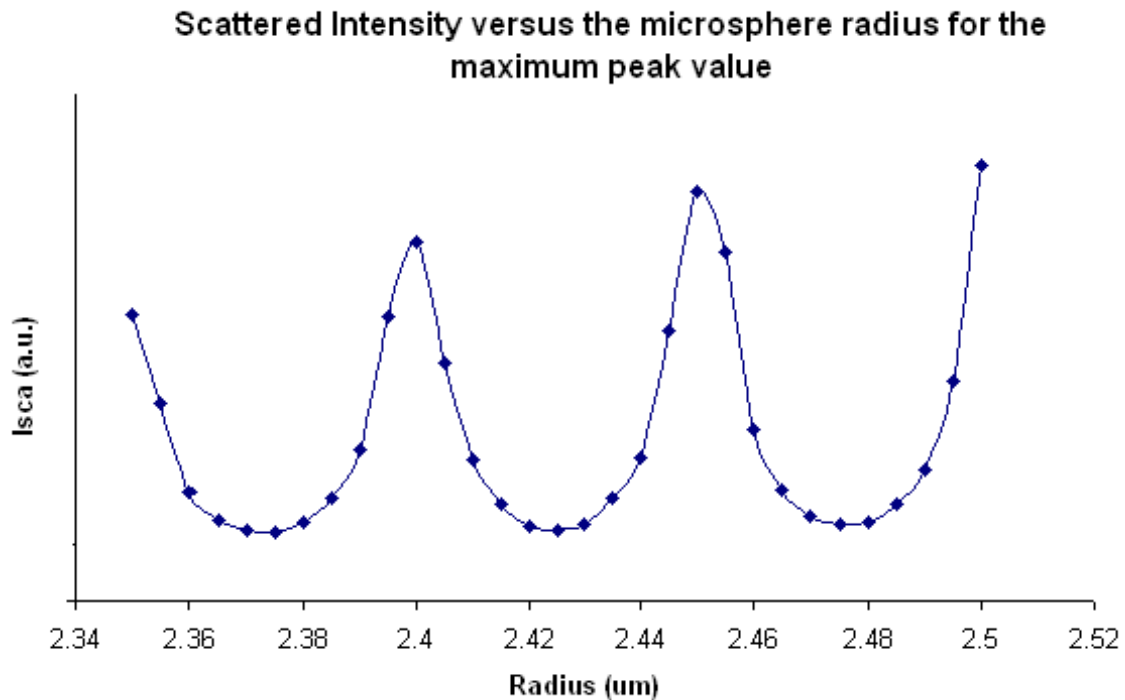
Figure 7 Plot of microsphere radius versus scattered intensity for a polydispersed PS sample in water. The data points are shown here for the maximum peak value. Here the data points are the calculated values and the curve is a fit.

For the microspheres, the number of vector spherical harmonics needed increases rapidly with microsphere size. Thus, the number of modes, l and m (mode number and azimuthal number) increases rapidly. The values of l and m define expansion coefficients required for the scattering field as well as for the incident field. For smaller microspheres small number of l are sufficient.

The code just not produced the values when those coefficients were not sufficient to generate the scattered field and hence by checking those values empirically, following values of l were introduced in the code.

- l is chosen as 159 for any values of microsphere size a, greater than 5 µm radius,

- for a < 5 µm, the value is 139 µm.

- for a < 3.45 µm the l is 99,

- for a < 2.45 µm, l is 79,

- for a < 1 µm, l is 49,

- for a < 0.3 µm, l is 27 and for any values of a < 0.3 µm the values is 17. The m values varies from $-l$ to $+l$

To determine the required step size, the scattered intensity was calculated for different step sizes across the YZ plane. Figure 8 shows that the calculated scattered intensity converges at step sizes below 125 µm. The light is collected across the YZ collection plane in steps of 100 µm.
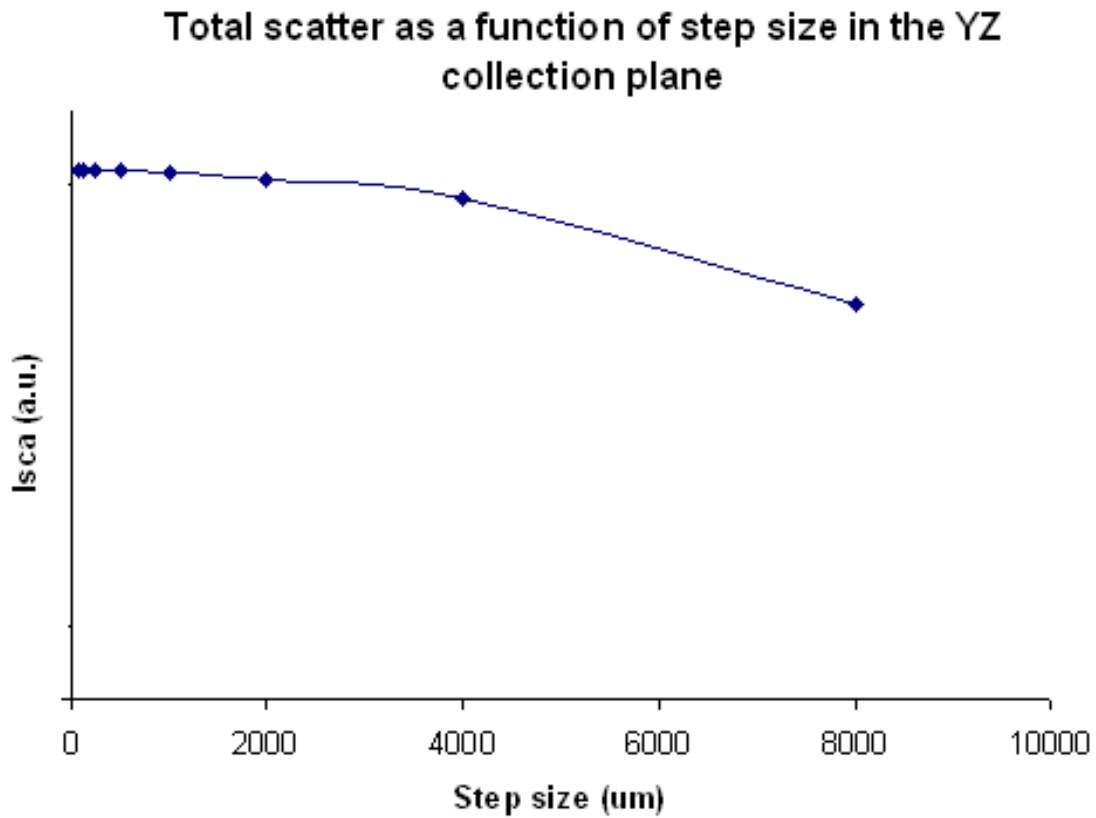
Figure 8 The total scattered intensity versus step size considered was calculated for a microsphere diameter of 1 μm. This convergence pattern holds for larger microspheres as well.

3.   Angular Scattering

The observation cone of interest is determined by the numerical aperture of the objective lens used for the experiment. For the theoretical calculations, this angle is taken to be 30º as seen in the theoretical section above. Figure 9 shows the scattered intensity with angle in the XZ plane. The region of interest for the DCPM system is from 60˚ to 120˚ where 0˚ is forward scattering and 180˚ is backward scattering. Within our

area of interest, the dominant scattering occurs in the forward scattering direction with a smaller peak appearing in the backward scattering direction. Since forward scattering is more intense than backward scattering, we observe a peak of higher intensity in that region. As seen in the experimental image, figure 5 the strong forward scattering results in the bright spot and the backward scattering may yield a dim spot on the other side of the microsphere. From this plot we can see that along with forward and backward scattering there is also light being scattered across the entire numerical aperture. So scattered light intensity is calculated and integrated across the entire field.
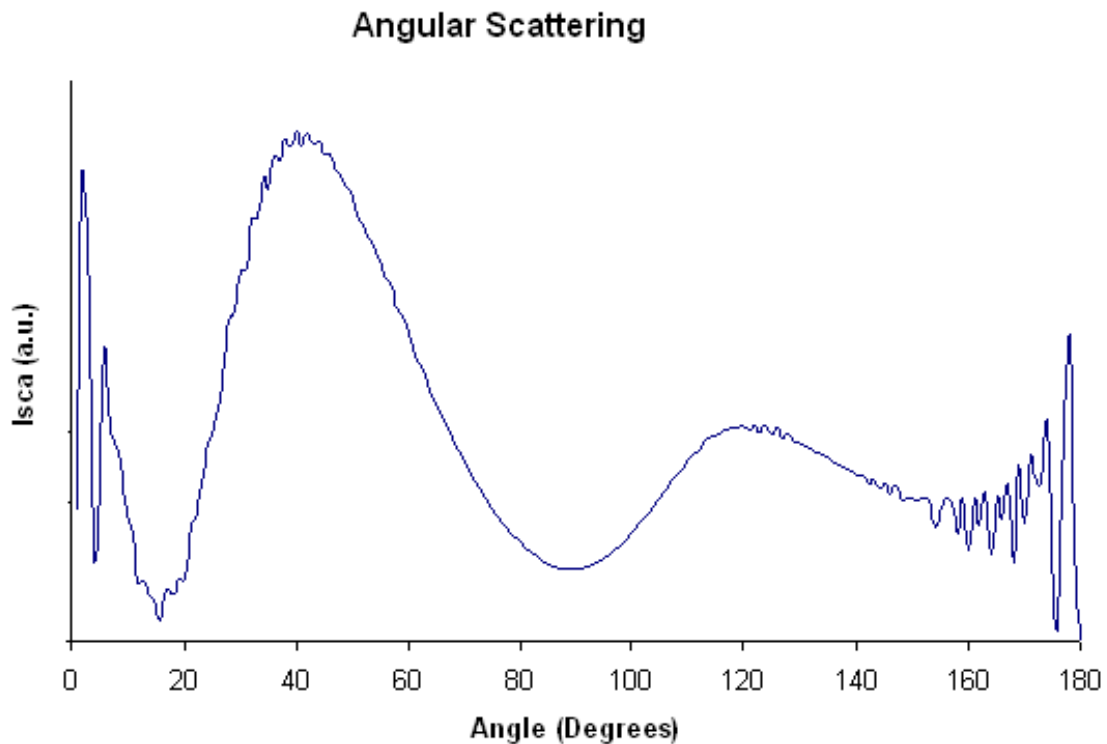

Figure 9 Angular scattering for microspheres in water and perpendicularly polarized incident light. These are the simulation results for 3 μm radius polystyrene microsphere in water.

RESULTS AND DISCUSSIONS

1.   Separation Distance and Scattered Intensity

To investigate the expected exponential decay of the scattered intensity with distance from the interface, the scattered intensity was calculated as a function of separation distance (d-a) between the microsphere and the interface. The results are shown in figure 10. It is anticipated that the scattered intensities from the microsphere will show an exponential decay following that of the incident evanescent waves. Scattered intensities are plotted for a microsphere with a diameter of 4 μm. However, the same dependence has been shown for microspheres of other sizes. If the graph is plotted for the separation distance in logarithmic scale, the slope of the theoretical calculated values should produce a value which is equal to β, the decay length of the evanescent wave. The calculated value of approximately 88 nm matches the experimental conditions. So, this theoretical study indicates that scattered intensity follows the decay of the incident evanescent waves being light.

Figure 10 Separation distance versus scattered intensity for the microsphere of size 4 m mean diameter in air. The separation distance is (d-a) and wavelength of incident light is 488 nm.

2.   Simulations

Calculations were performed for microsphere samples with mean diameters of the 1 and 4 µm to study the effects of polydispersity on the scattering intensities. The steps taken for the radius were 5 nm. All the other parameters considered for theoretical

calculations are as described in the theoretical calculations section. Thus there are no free parameters in the calculation except for the microsphere radius.

3.   1 µM Radius of the Microsphere

The total scattered intensity collected at height of 2 mm, for microspheres around 1 µm diameter are shown in figure 11. As expected, the scattered intensity increases as the size of the microsphere increases. In this size range, the scattered intensity can increase by up to a factor of two with only a 200 nm microsphere size difference.
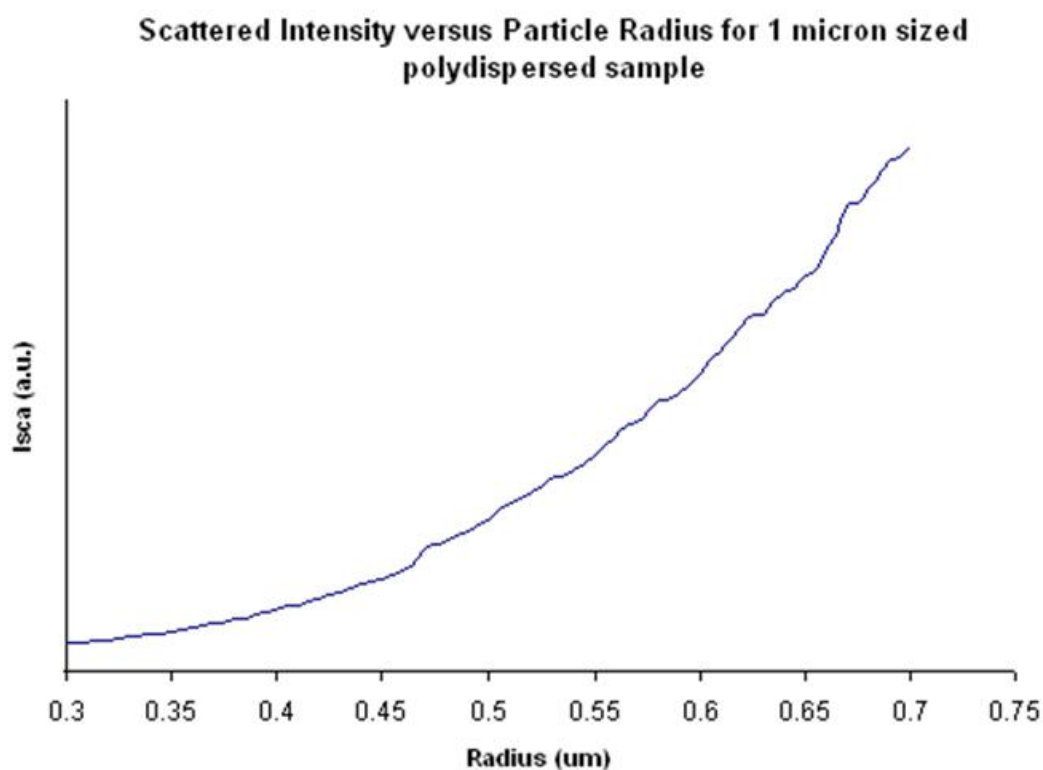

Figure 11 Scattered intensity in arbitrary units (a.u.) versus microsphere size of 1 µm polydispersed PS sample when excited by evanescent waves.

The stuck particle scattering intensity data was experimentally collected by the Bevan laboratory using the technique described in the experimental section.[47] In order to avoid errors, the data were averaged in 40 continuous snapshots. Also the concentration prepared was very dilute in order to avoid interfering signals from neighboring microspheres.

Since the microsphere sample is polydisperse, the size distribution was measured and shown in figure 12(a) by dashed lines and circles. With the help of Confocal Laser Scanning Microscopy (CLSM), the microspheres are seen and their corresponding sizes are determined by measuring the diameter of the microspheres. The image is then processed and with the help of fourier Radius values are used to calculate the number of microspheres in each bin selected. So, the points in this plot show the number of microspheres present in a sample of the same microspheres used in the experiment. Note that this is not a characterization of the same microsphere sample used in the DCPM system. This produces the plot of size distribution. The solid line in the same plot depicts the scattered intensity values calculated theoretically over the size distribution range of the 1 μm sample.

To compare the experimental data with theoretical calculation, scattering intensity data particle histograms are created as shown in the figure 12(b). For easy comparison, both the histograms are shown as normalized frequencies (f_i) and normalized intensities (I/I_m). Where the plots are normalized to maximum frequency and most probable intensity (I_m) as shown in the plot 12 (b). The experimental scattered intensity is shown

with the dashed lines and circles. The theoretically calculated scattered intensity was combined with the experimental size distribution to yield the solid curve. The histogram of the theoretical scattered intensity values was created by dividing the intensity distribution into bins that are equally spaced. Since there is 1500 data points for each experiment the number of bins chosen are 50.

The theoretical results qualitatively match the experimental results. The normalized intensity results show a tail toward lower scattered intensities due to the tail toward smaller diameters in the size distribution. The calculated intensity distribution is a bit broader than the measured intensity distribution. It is possible that the size distribution of the characterized sample did not exactly match that of the sample used to determine the size distribution. Also for the calculations boundary conditions and surface reflections are neglected. However, these calculations qualitatively predict the scattered light intensity distribution from a polydisperse microsphere sample with a mean diameter of about 1 µm.
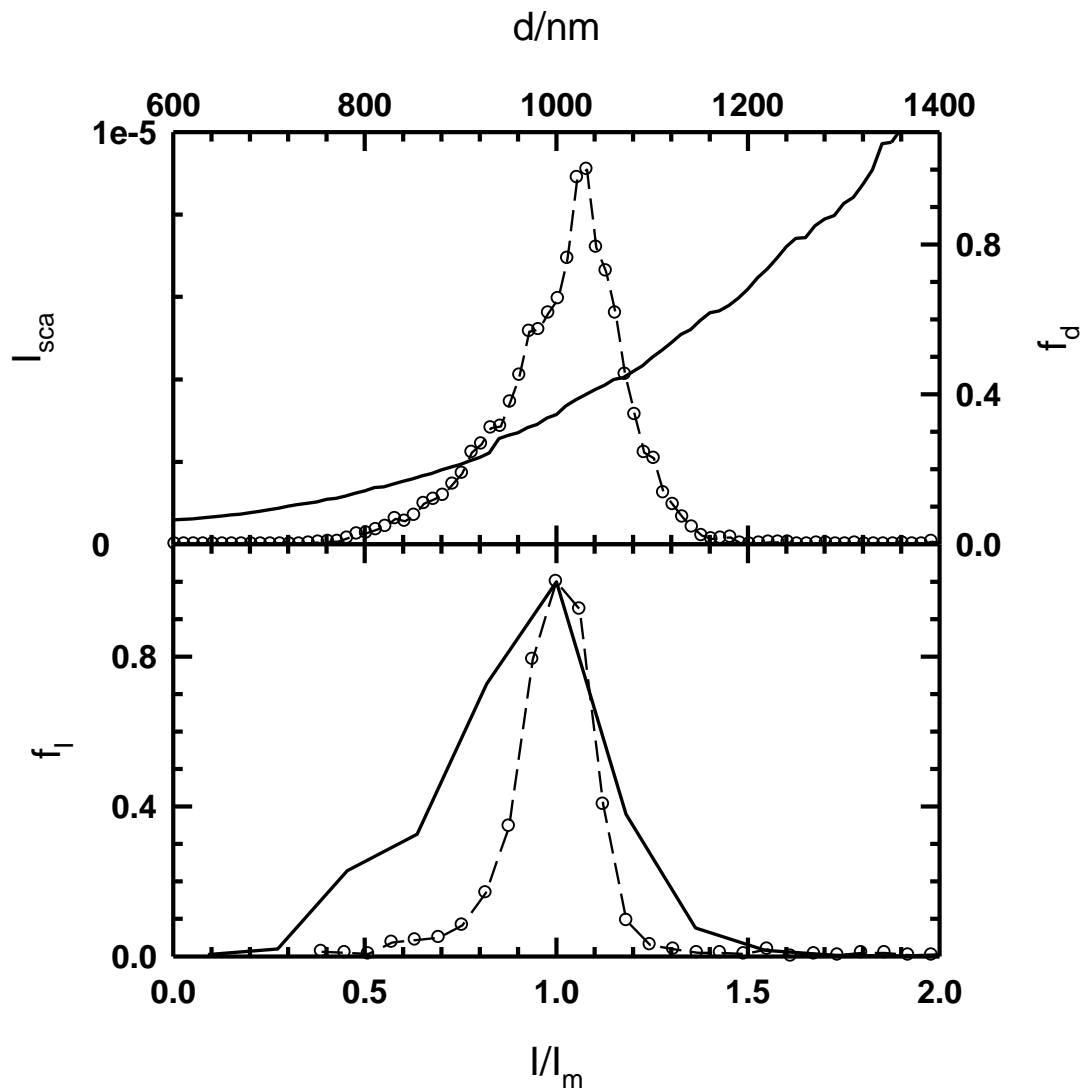
Figure 12 Comparison of values with experimental data for 1μm size distribution and scattering intensity of 1μm PS microspheres. (a) The solid lines represent the theoretical calculated values. For the size distribution plot the frequency (fd) of microspheres are normalized to most probable frequency. (b) The histograms of scattering intensity obtained by theoretical calculations (solid lines) and experimental measurements (dash lines).

4.   4 µM Radius of the Microsphere

Figure 13 is the plot of the theoretically calculated scattered intensity versus the microsphere radius for 4 µm size. Here scattering intensity variations calculated by modified Mie theory show oscillation behavior which are sharper than those in for 1 µm. Also the sharp peaks indicate the development of weak resonances. As described before, in the section of mie as well in the section of WGM, larger microspheres or those in media with a higher effective refractive index such as microspheres suspended in air instead of water, would cause the occurrence of resonance peaks. Thus the oscillatory behavior is seen in the microspheres of larger particle sizes and also these oscillations are correspondingly more if the microspheres are seen in water instead of air. Water reduces the effective refractive index calculated and hence we observe this pattern.

The comparison of the experimental and theoretical values is as shown in the figure 14 (b). As in the previous results, figure 14(a) shows the size distribution (open circle) and theoretical intensity variation (solid line) for 4 µm PS microsphere. 4 µm are more polydispersed than 1 µm PS microspheres. The values again match fairly well and the variations may be attributed to the errors in the experiments as mentioned in the discussion of 1 µm microspheres. The variations can be due to the experimental errors. 4 µm PS sample is more polydispersed than 1 µm and hence there is a possibility that entire sample is not considered for the size distribution calculations here. Again here also the boundary conditions are neglected and hence surface reflections are not taken into consideration. A long tail to the high intensity side is observed in the scattered

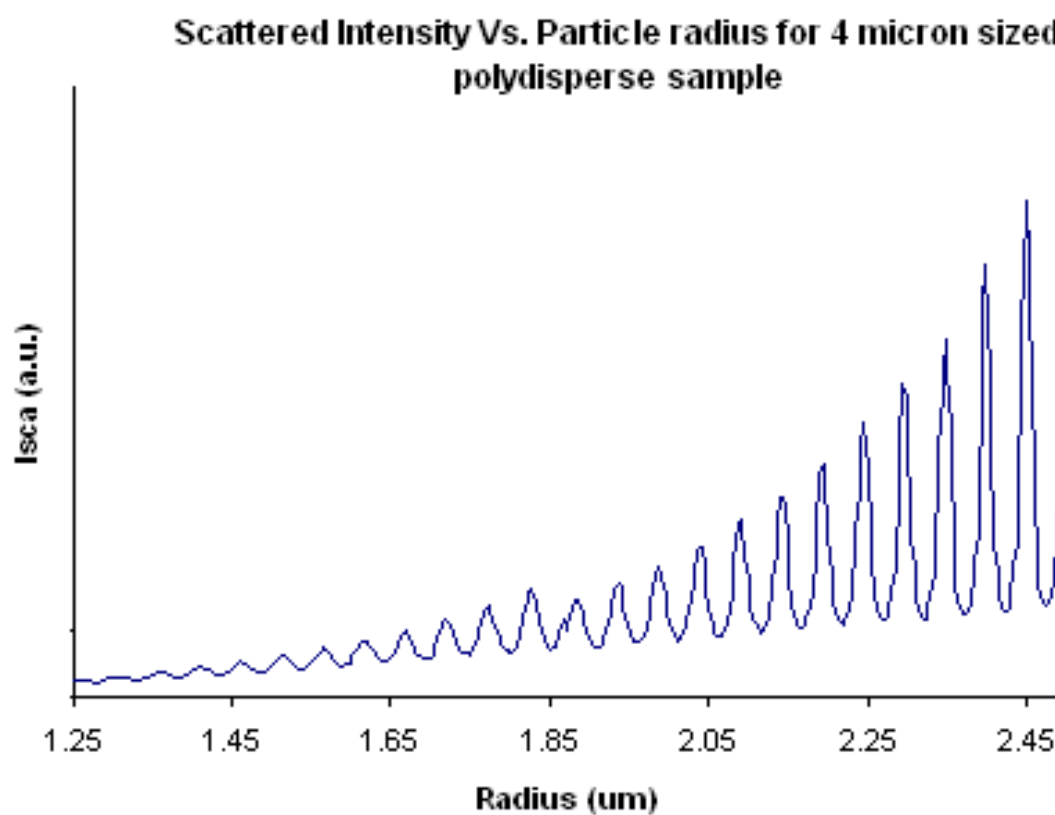intensity values in figure 14 (b). This may be due the larger number of large microspheres in the polydispersed sample of 4 µm.

Figure 13 Scattered intensity in arbitrary units (a.u.) versus microsphere size of 4 µm polydispersed PS sample when excited by evanescent waves.
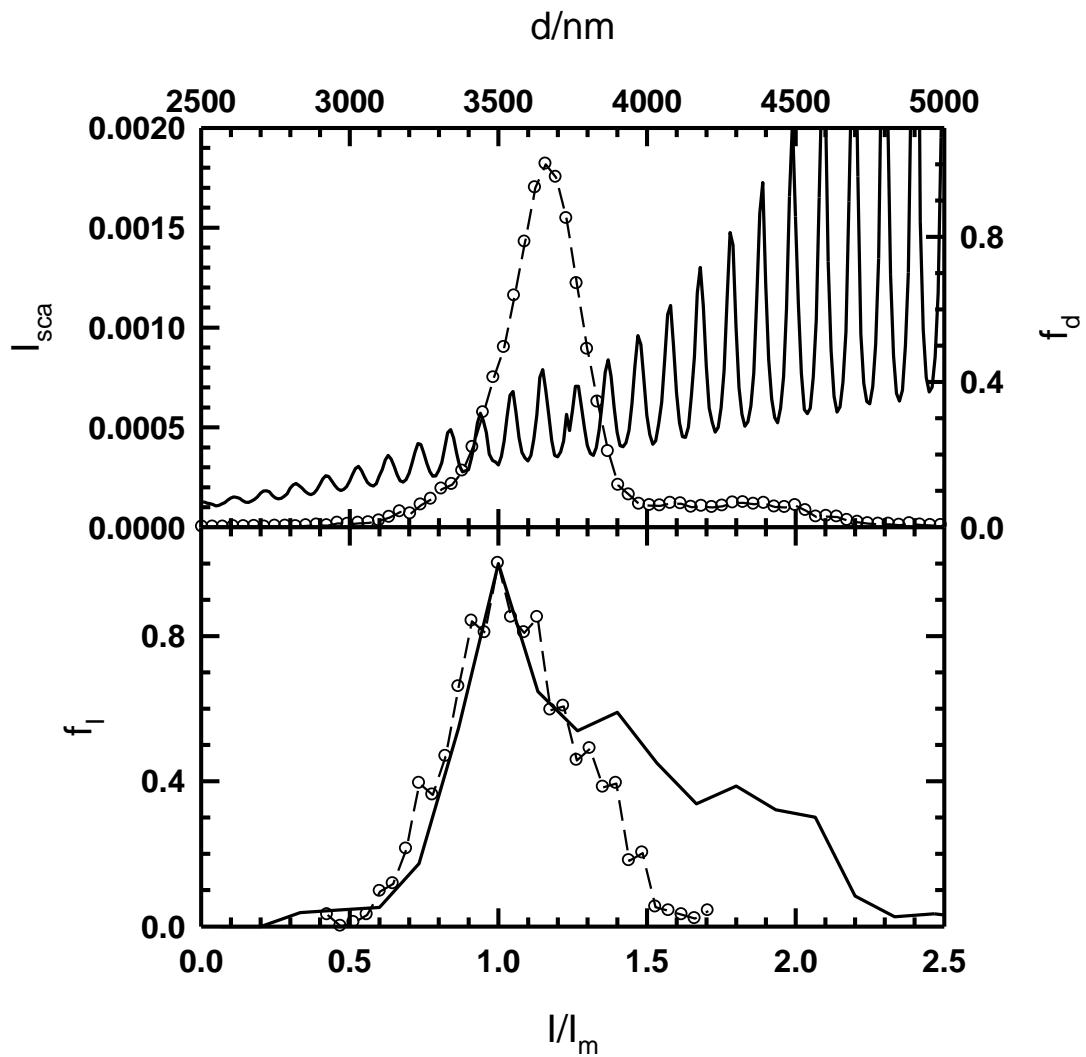
Figure 14 Size distribution and scattering intensity of the 4 μm polydispersed microsphere sample size distribution and scattering intensity of 4μm PS microspheres. (a) The solid lines represent the theoretical calculated values. For the size distribution plot the frequency (fd) of microspheres are normalized to most probable frequency. (b) The histograms of scattering intensity obtained by theoretical calculations (solid lines) and experimental measurements (dash lines).

5.   WGM Results

To investigate WGMs in the DCPM system, the scattered intensity was calculated for polystyrene microspheres of approximately 3 µm in air. Choosing air as the medium provides additional confinement for the WGMs increasing effective refractive index, and causes the WGMs to occur at smaller size parameters. Figure 15 shows the results of these calculations. A sharp peak is observed at a radius of approximately 3.25 µm. Thus when a polydisperse microsphere sample of approximately this diameter is observed under DCPM, some microspheres should exhibit WGMs. Since the peaks are narrow, only a few microspheres are expected to show this effect. To predict what the microsphere should look like in the DCPM system, angular distributions for microspheres with a WGM (blue) and without a WGM (magenta) are plotted in Figure 16. The exact sizes for the microspheres are indicated on figure 15. There are distinctively more features in the scattered intensity for the microsphere with the WGM than the microsphere without the WGM. In terms of the DCPM system's collection cone from 60º to 120 º, the collected scattered light is significantly higher and should be visible across the entire microsphere instead of at the front and back as seen in microspheres without WGMs.
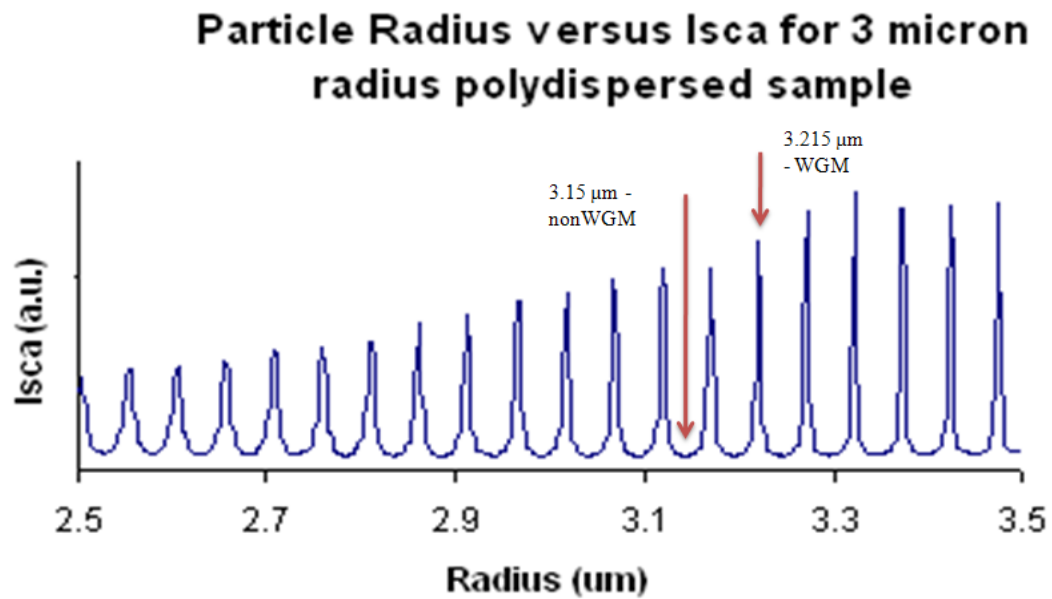
Figure 15 Theoretical calculation results for the microsphere size vs. scattered intensity for polydispersed PS microspheres in air with mean diameter of 6 μm.
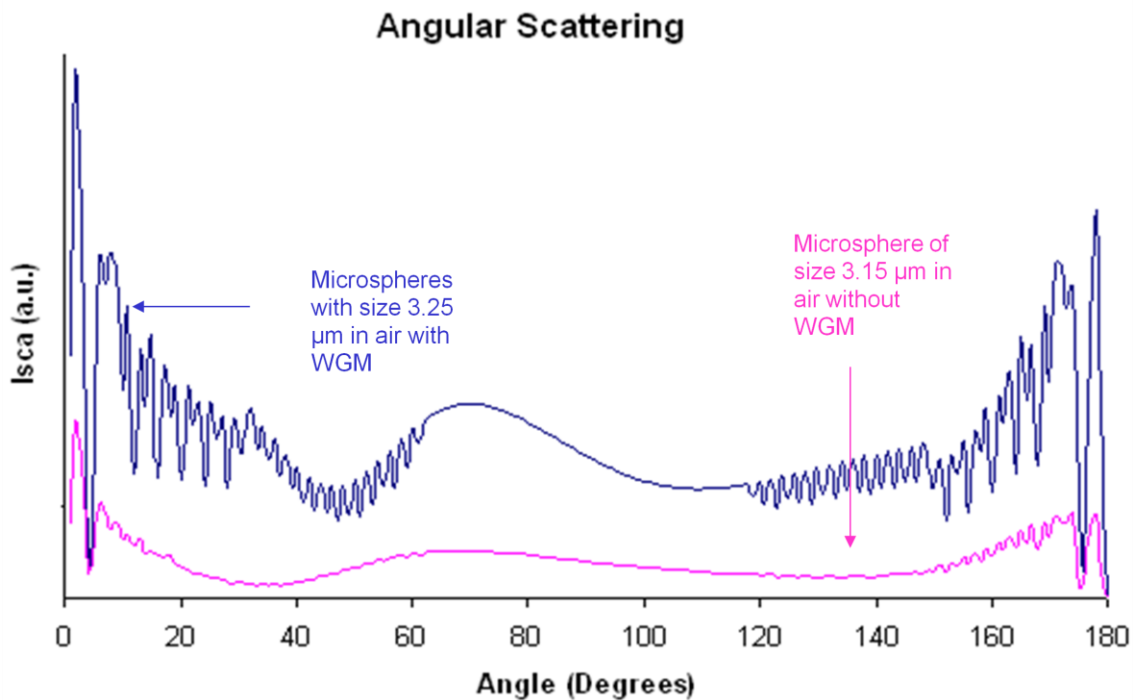

Figure 16 The angular scattering pattern for the microspheres of mean diameter 6 μm for PS microspheres in air. 3.25 μm is the WGM and 3.15 μm is the microsphere without WGM.

To experimentally observe WGMs, stuck intensities were imaged for polystyrene microspheres of radius 3 μm with CV of 5.1%. Experimental images for the microspheres in air produced the results shown in figures 17 and 18 with the evanescent light traveling from left to right. Figure 17 is an image in air with only scattered light. Figure 18 is a backlit image with scattered light. Here, one of the microspheres produced significantly more scattered intensity than similar-sized microspheres. As seen in the figure this microsphere scatters light throughout the equatorial surface. For all the other spheres distinct forward scattering and some back scattering are observed as expected.

The differences in these scattering patterns are consistent with those predicted by the theoretical model for a WGM. It is clear that the microsphere of interest is different than the other microspheres and the scattered light distribution indicates that it could be supporting a WGM. However, we cannot say for sure because we are not able to tune across the WGM with the laser wavelength. The appearance and use of WGMs could open the technique to biosensing applications. The details are mentioned in the section of biosensing before. It can be used to sense the biomolecules like proteins, peptides attached on the surface of the microsphere from the shift of wavelength[48].
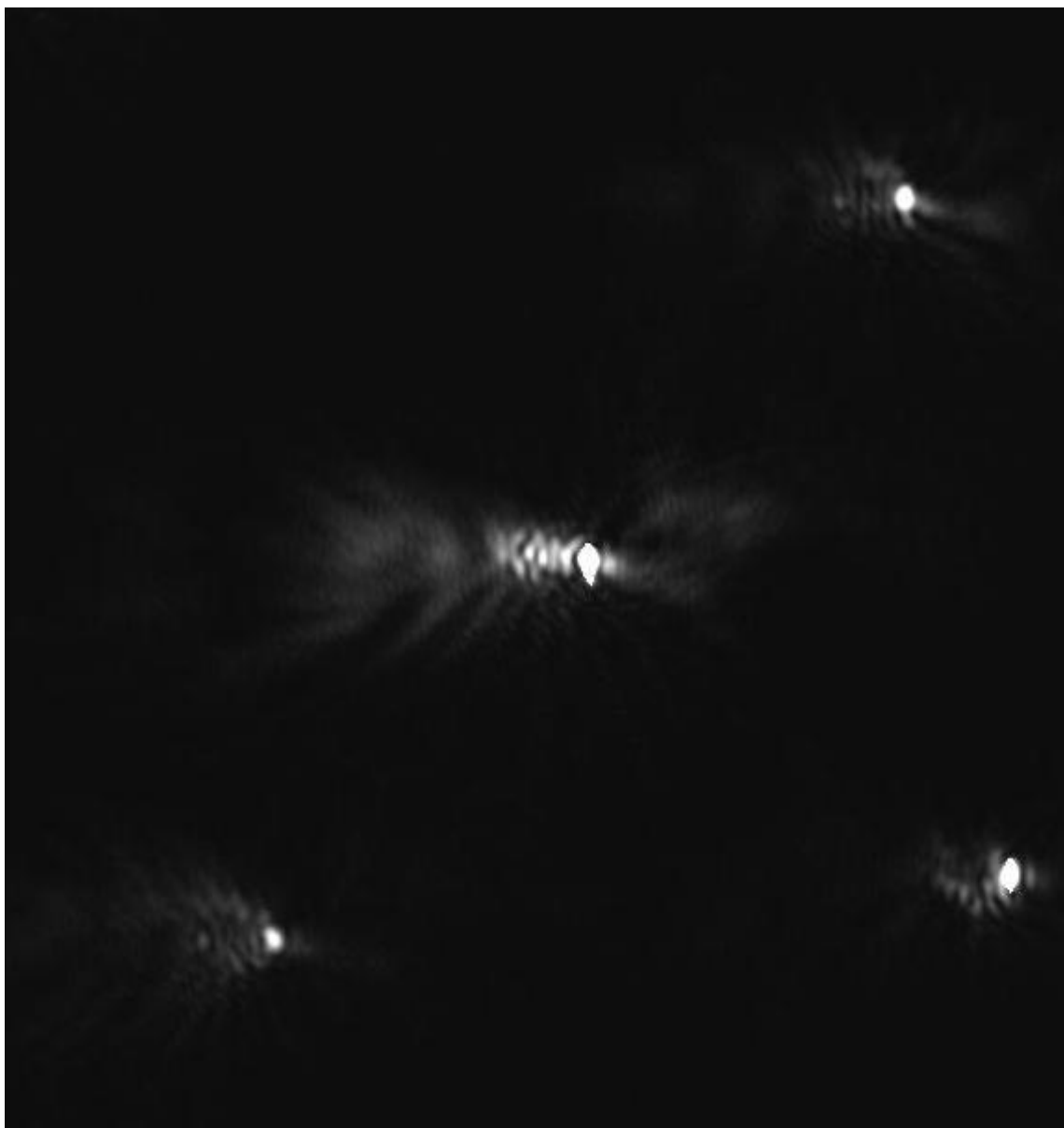
Figure 17 Scattering from approximately 6 micron polystyrene microspheres in air without any background light.
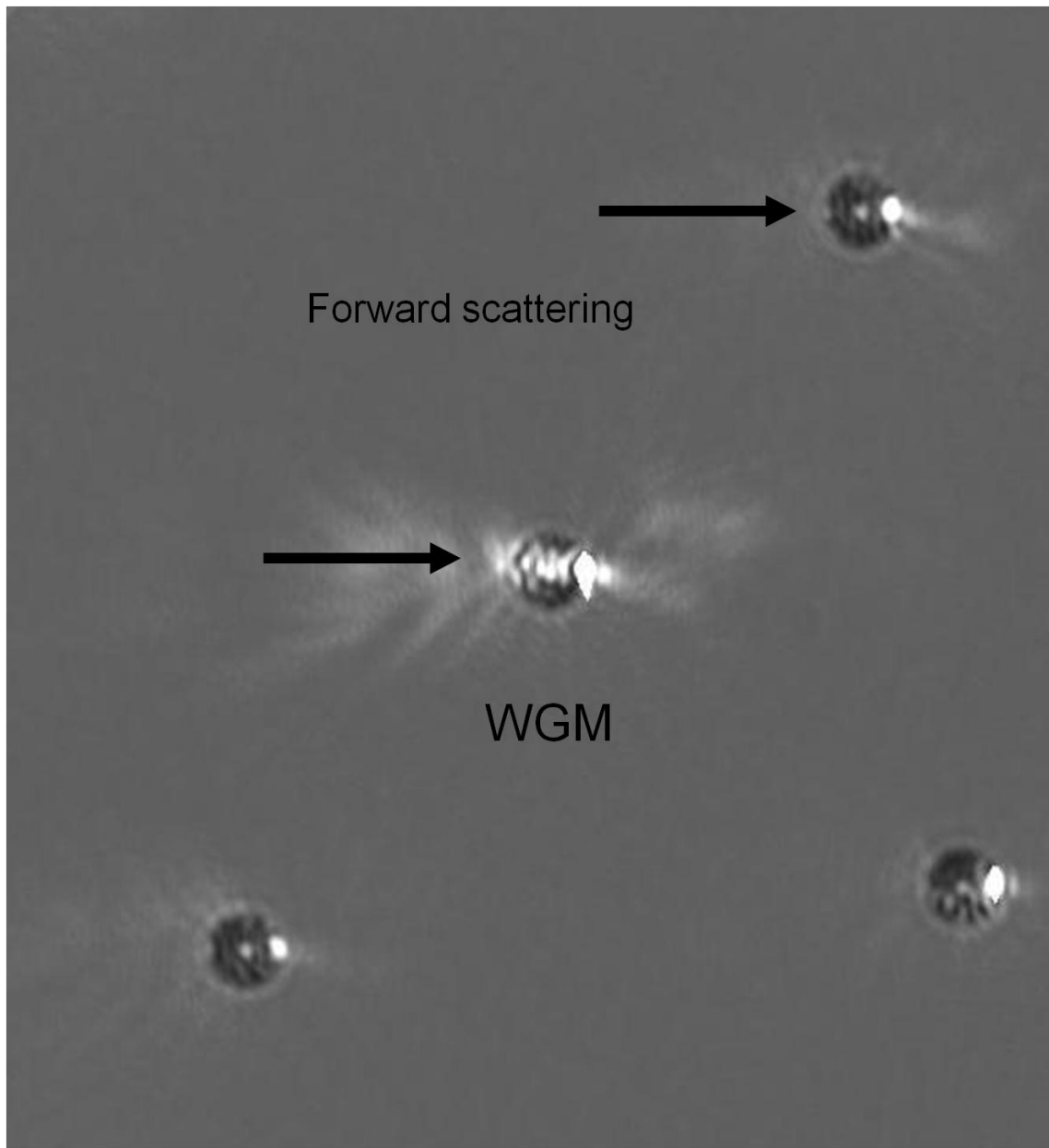
Figure 18 Scattered light from around 6 micron diameter polystyrene microspheres in air with background light.

SUMMARY AND FUTURE WORK

This work demonstrated that modified Mie theory can be used for modeling scattered intensity from a polydisperse sample of microspheres in an evanescent field. The modified Mie theory accounted for the exponential decay of the evanescent field away from the glass-water interface. In addition to the height above the surface, the scattered intensity was found to be highly dependent upon the microsphere size and index of refraction, and the index of refraction of the surrounding medium. Scattered intensity values were calculated for a range of polystyrene microspheres. Using a experimentally determined microsphere size distributions for samples with nominal diameters of 1 μm and 4 μm, and the calculated scattered intensity values for each microsphere size, the distribution of scattered intensities was calculated for each of the samples. These distributions were then normalized to the most probable scattered intensity and compared to experimentally collected data. The theoretical data qualitatively matched the experimental scattered intensity distribution. This indicated that scattering differences due to microsphere size play a role in the distribution of scattered intensity observed in polydisperse microsphere samples. Through understanding the physical mechanism behind the distribution, techniques using multiple microsphere probes simultaneously, such as DCPM, may be improved or modified to yield lower experimental error. Such a system would be extremely useful in the study of biomolecular interaction in the sub-picoNewton range.

Future work will include additional calculations for different microsphere size ranges and the inclusion of boundary effects, such as surface reflection from the glass, in the calculation. Additionally, the FORTRAN code should be modified to include automatic adjustment of the number of spherical harmonics required to produce accurate results for each microsphere size. At this time, the parameter is manually adjusted and must be checked through convergence plots.

An initial investigation into the use of WGMs in a DCPM system was performed. Calculations indicated the appearance of narrow WGMs in larger-sized microspheres (approximately 6 μm diameter) when excited in air. Total scattered light intensity and scattered light intensity as a function of angle were calculated. Experimental data was collected from a polydisperse microsphere sample with a mean diameter of 6 μm in air. A small number of microspheres produced a scattered intensity pattern similar to that of a WGM. Unfortunately the current DCPM cannot be used to positively determine the existence of a WGM due to the fixed wavelength excitation. However, we believe it is possible to produce WGMs in such a DCPM system. These resonant modes could be utilized as refractometric sensors and greatly extend the utility of the DCPM system by incorporating a sensing component. To accomplish this goal, a tunable laser must be coupled to the DCPM system.

REFERENCES

1. Zvyagin, A. V.; Goto, K., *Optical Society of America* **1998**, *15*, 3003.

2. Xiaoyan, M.; Jun Qing, L.; Huafeng, D.; Xin-Hua, H., *Optics Letters* **2005**, *30*, 412.

3. Cheng, D. K. *Fundamentals of Engineering Electromagnetics*. Prentice Hall: **1993**.

4. Ganic, D.; Gan, X.; Gu, M., *Optics Communications* **2003**, 216, 1.

5. Allen, A. Modeling scattered intensities for multiple particle TIRM using Mie theory. Texas A&M University, College Station, **2006**.

6. Chew, H.; Wang, D.-S.; Kerker, M., *Applied Optics* **1979**, *18*, 2679.

7. Ganic, D.; Gan, X.; Gu, M., *Optik Optics* **2002**, *113*, 135.

8. Prieve, D. C., *Advances in Colloid and Interface Science* **1999**, *82*, 93.

9. Prieve, D. C.; Walz, J. Y., *Applied optic* **1993**, *32*, 1629.

10. Liebert, R. L. B.; Prieve, D. C. *Biophysics* **1995**, *69*, 66.

11. Robertson, S. K.; Uhrick, A. F.; Bike, S. G. *Journal of Colloid Interface science* **1998**, *202*, 208.

12. Bike, S. G., *Colloid and interface science* **2000**, *5*, 144.

13. Rudhardt, D.; Bechinger, C.; Leidere, P., *Physics Review letter* **1998**, *81*, 1330.

14. Rudhardt, D.; Bechinger, C.; Leiderer, P., *Journal of Physical condensed matter* **1999**, *11*, 10073.

15. Binnig, G.; Quate, C. F., *Physical Review Letter* **1986**, *56*, 930.

16. Lee, C.-K.; Wang, Y.-M.; Huang, L.-S.; Lin, S., *Micron* **2006**, *38*, 446.

17. Jeong, K.-H.; Keller, C.; Lee, L., *Applied Physics Letter* **2005**, *86*, 193901-1.

18. Allen, S.; Chen, X.; Davis, J.; Davies, M.; Dawkes, A.; Edwards, J.; Roberts, C.; Sefton, J.; Tendler, S.; Williams, P. *Biochemistry* **1997**, *36*, 7457.

19.   Lee, G.; Chrisey, L.; Colton, R., *Science* **1994**, *26*, 771.

20.   Ashkin, A., *Methods Cell Biology* **1998**, *55*, 1.

21.   Williams, M., Optical Tweezers: Measuring Piconewton Forces. In NorthEastern University: Boston, p 13.

22.   Tinoco, I. J.; Li Pan, T. X.; Bustmante, C., *Quarterly Reviews of Biophysics* **2006**, *39*, 325.

23.   Finer, J.; Simmons, R.; Spudich, J., *Nature* **1994**, *368*, 113.

24.   Fallman, E.; Schedin, S.; Jass, J.; Andersson, M.; Uhlin, B. E.; Axner, O., *Biosensors and Bioelectronics* **2004**, *19*, 1429.

25.   Camesano, T. A.; Liu, Y.; Datta, M., *Elsevier* **2007**, *30*, 1470.

26.   Dufreˆne, Y. F., *Curr. Opin. Microbiol.* **2003**, *6*, 317.

27.   Vadillo-Rodriguez, V.; Busscher, H. J.; Norde, W.; de Vries, J.; Dijkstra, R. J. B.; Stokroos, I. e. a., *Applied Environmental Microbiology* **2004**, *70*, 5541.

28.   Ashkin, A.; Dziedic, J. M.; Bjorkholm, J. E.; Chu, S., *Optics letters* **1986**, *11*, 288.

29.   Prieve, D. C., *Advances Colloidal Interface Science* **1998**, *82*, 93.

30.   Wannemacher, R.; Pack, A.; Quinten, M., *Applied Physics B* **1999**, *68*, 225.

31.   Bohren, C. F.; Huffman, D. R., *Absorption and Scattering of Light by Small Particles*. Wiley-Interscience: **1983**.

32.   van de Hulst, H. C., *Light Scattering by Small Particles*. Dover Publications Inc.: **1981**.

33.   Shankarapandian, M. *Spectral multiplexing using quantum dot tagged microspheres with diffusing colloidal probe microscopy*. Texas A&M University, College Station, **2007**.

34.   Everett, N. W.; Wu, H.-J.; Anekal, S.; Sue, H.-J.; Bevan, M., *Biophysical Journal* **2007**, *92*, 1005.

35.   White, I. M.; Hunumegowda, N. M.; Fan, X., *Optics letters* **2005**, *30*, 3189.

36.   Matsko, A. B.; Ilchenko, V. S., *IEEE Journal Sel. Top. Quantum Electron* **2006**, *12*, 3.

37.   Jory, M. J.; Perkins, E. A.; Sambles, R. J., *Optical Society of America* **2003**, *20*, 1785.

38.   Arnold, S.; Khoshsima, M.; Teraoka, I., *Optics letters* **2003**, *28*, 272.

39.   White, I. M.; Zhu, H.; Suter, J.; Hunumegowda, N. M.; Oveys, H.; Zourab, M.; Fan, X., *IEE Sensors Journal* **2007**, *7*, 28.

40.   Quan, H.; Guo, Z., *Journal of Quantitative Spectroscopy & Radiative Transfer* **2005**, *93*, 231.

41.   Barber, P. W.; K, C. P., *Optical Effects Associated with Small Particles*. World Scientific: Singapore, **1988**.

42.   Vollmer, F.; Braun, D.; Libchaber, A., *Applied Physics Letters* **2002**, *80*, 4057.

43.   Vollmer, F.; Arnold, S.; Braun, D.; Teraoka, I.; Libchaber, A., *Biophysical Journal* **2003**, *85*, 1974.

44.   Ganic, D. *Far field and near field optical trapping*. Swinburne University of Technology, Melbourne, Australia, **2005**.

45.   Wu, H.-J.; Bevan, M., *Langmuir* **2005**, *21*, 1244.

46.   Wu, H.-J.; Pangburn, T. O.; Beckham, R.; Bevan, M., *Langmuir* **2005**, *21*, 9879.

VITA

Suhani Kiran Shah received her Bachelor of Engineering degree in instrumentation and control engineering from the Nirma Institute of Technology, Gujarat University in 2005 and received her Master of Science degree in biomedical engineering in December 2007 from Texas A&M University.

Ms. Suhani may be reached at 331/Lane 17, Satyagraha Chhavani Society, Satellite Road, Ahmedabad – 380015. Her Email address is suhani.shah9@gmail.com.